CERN-ACC-2020-0011
roderik.bruce@cern.ch

HL-LHC operational scenarios for Pb-Pb and p-Pb operation

R. Bruce, T. Argyropoulos, H. Bartosik, R. De Maria,
N. Fuster-Martinez, M.A. Jebramcik, J.M. Jowett*, N. Mounet,
S. Redaelli, G. Rumolo, M. Schaumann, H. Timko
CERN, Geneva, Switzerland.

Abstract

This report describes the running scenario for operation with Pb-Pb and p-Pb collisions in the HL-LHC. The expected beam parameters are described, starting from the beams delivered from the injectors, as well as possible filling schemes. The machine configuration is also discussed, in terms of optics and settings of critical components such as collimators. Finally, the future luminosity performance in typical fills for Pb-Pb and p-Pb collisions is simulated, and the expected integrated luminosity over the HL-LHC physics programme is calculated and compared to the requirements from the experiments.

Geneva, Switzerland
29 July 2020

*Now at GSI Helmholtzzentrum für Schwerionenforschung, Darmstadt, Germany.

Contents

1 Introduction

The LHC Design Report [1] foresaw a heavy-ion programme whose scope was limited to Pb-Pb collisions in two of the LHC experiments at a time, one of which was the specialised ALICE [2] detector. The luminosity was expected to be limited around the design value of 1×10^{27} cm^{-2}s^{-1} by the bound-free pair production effect at the collision points. In addition, the Pb beam intensity was expected to be limited by the capabilities of the injectors, intra-beam scattering, and a reduced collimation efficiency with respect to protons, arising from the more complicated nuclear interactions of heavy-ion beams with the collimators. An integrated luminosity goal of 1 nb^{-1} was set for the first 10 years of Pb-Pb operation [2].

Except that 3 experiments took data simultaneously from the beginning, this mode of operation was implemented very successfully in Run 1 (2010–2013) [3]. As the physics output grew richer and ever more surprising, the scope of the heavy-ion programme expanded dramatically (see below) to include all the LHC experiments (ALICE, CMS, ATLAS, LHCb and, occasionally, LHCf). In Run 2 (2015–2018) [4, 5, 6], the beam energy was increased and the performance limits expected at the time of the Design Report were overcome, resulting in a Pb-Pb luminosity exceeding 6 times the original design value.

Four Pb-Pb runs have taken place to date (in 2010, 2011, 2015, and 2018), resulting in a total integrated luminosity of about 1.5 nb^{-1} at ALICE, thus surpassing the initial target despite the beam energy (3.5 Z TeV in Run 1 and 6.37 Z TeV in Run 2) being lower than nominal and more experiments sharing luminosity. So far, ALICE was levelled at 1×10^{27} cm^{-2}s^{-1} in order not to exceed the event rate limit of the detector. ATLAS and CMS collected in total about 2.5 nb^{-1} in Run 1 and Run 2, since they could run at higher luminosity [7]. LHCb was the last experiment to join the heavy-ion programme, integrating about 0.25 nb^{-1} in Run 2.

In addition to Pb-Pb collisions, a completely new mode of operation with proton-nucleus collisions was implemented [8, 9, 10, 11]. Following a one-day pilot run in 2012, extended physics runs with p-Pb were carried out in 2013, and 2016, which were not foreseen at the LHC design stage. About 250 nb^{-1} were gathered in ATLAS and CMS, and 75 nb^{-1} in ALICE.

The heavy-ion programme is scheduled to continue in Run 3 and Run 4. We do not discuss the planning of the schedule year-by-year but focus on the potential performance in a typical one-month annual run *entirely devoted* to Pb-Pb or p-Pb collisions.

The LHC performance in these runs will benefit from upgrades of the LHC injectors [12] and upgrades included in the high-luminosity LHC (HL-LHC) project [13]. All upgrades of the injectors, collider, and experiments relevant to the

	Pb-Pb (nb^{-1})	p-Pb (nb^{-1})
ALICE	13	600
ATLAS	13	1200
CMS	13	1200
LHCb	2	600

Table 1: Integrated luminosity requested by the LHC experiments for Pb-Pb and p-Pb operation until the end of Run 4 [14, 18].

heavy-ion programme are planned to be implemented during long shutdown 2 (LS2), making the full heavy-ion "HL-LHC" performance available already in Run 3. In the planning as of 2019, it was foreseen to do four future Pb-Pb runs, one p-Pb run, and one short p-p reference run.

The overall goals of the Run 3–4 programme were initially set according to [14]. The central component was the accumulation of 10 nb^{-1} of Pb-Pb luminosity in the ALICE experiment between LS2 and LS4, with an additional 3 nb^{-1} at a lower magnetic field, assuming a (levelled) peak hadronic interaction rate of 50 kHz [14, 15, 16, 17], which corresponds to a levelled luminosity of about 6.4×10^{27} $\mathrm{cm}^{-2}\mathrm{s}^{-1}$. To have some margin in the design of protection against beam losses, we assume that levelling could be done up to 7×10^{27} $\mathrm{cm}^{-2}\mathrm{s}^{-1}$. A similar luminosity would be delivered to ATLAS and CMS with filling schemes adjusted to provide a somewhat smaller level to LHCb.

A proposal for an extended LHC heavy-ion programme was presented in 2018 as a part of the HL-LHC and HE-LHC workshop [18]. This proposal includes further heavy-ion runs beyond Run 4, including a programme for collisions of lighter nuclei. Luminosity requests for all LHC experiments for Pb-Pb and p-Pb operation until the end of Run 4 are also shown in [18], which we summarise in Table 1. In order to allow this amount of luminosity to be collected, [18] also proposed to extend the total running time during Runs 3–4.

In this report, we present operational scenarios for the Pb-Pb and p-Pb runs in Run 3 and Run 4. First, we discuss the beam parameters in Sec. 2 and then the configuration of the LHC machine in Sec. 3. We then estimate the future performance during a typical one-month run for Pb-Pb in Sec. 4 and for p-Pb in Sec. 4.4. In these sections, we estimate the integrated luminosity for a few different running scenarios, using tools now benchmarked in the LHC. Finally, we compare the projections with the requests from the experiments and discuss possible improvements.

	LHC design	2018	HL-LHC
Total no. of bunches	592	733	1240
Bunch spacing (ns)	100	75	50
no. of bunches per injection	54	42	56
Bunch intensity (10^7 Pb ions)	7	23	19
Normalized transverse emittance (μm)	1.4	n.a.	1.5

Table 2: Pb beam parameters at injection into the LHC at an energy of 450 Z GeV, as foreseen in the LHC design report [1], as achieved in 2018 [7, 6], and as envisaged for HL-LHC [19]. The parameters quoted for 2018 are directly at injection, before any blowup on the flat bottom; unfortunately there are no reliable measurements of the transverse emittance with 75 ns beams.

2 Beam parameters

2.1 LHC beam at injection

The Pb-beams that can be produced by the HL-LHC injectors complex were initially set out in [12], based on the experience from the 2015 Pb-Pb run. The estimate of achievable intensity was, however, lower than the HL-LHC requirements in [16]. Since then, significant work has been done in the injectors complex, and an improved Pb beam quality in the 2016 p-Pb run resulted in an updated and improved parameter set for the injected beams, which was presented in [19] and used in an updated HL-LHC Pb baseline [17]. We take these beam parameters as input for the studies in following sections. They are shown in Table 2, together with the LHC design values and what was achieved operationally in 2018.

For the 2018 run, the Pb beam production scheme was further improved [20], allowing for a larger number of bunches to be injected into the LHC than in 2016 thanks to a reduced bunch spacing (75 ns instead of 100 ns). The LHC could reach a peak luminosity just above 6×10^{27} cm^{-2}s^{-1} in 2018, with bunch intensities surpassing the HL-LHC requirements, although with fewer bunches. This peak value is close to the foreseen HL-LHC levelled luminosity.

In order to reach the HL-LHC parameters, the only remaining major injectors upgrade is the momentum slip-stacking in the SPS [12]. This relies on a new low-level RF system, which is being installed in LS2, that will interleave bunch trains to halve the bunch spacing. In [17, 19] it was shown that slip-stacking will increase the total number of circulating LHC bunches from 733, with 75 ns bunch spacing as in 2018, to 1232 bunches spaced by 50 ns. As discussed in the following section, the number of bunches can be increased to 1240 after optimisation of the abort gap keeper bucket number. In the event that slip-stacking is not available from the start of Run 3, due, e.g. to delays in commissioning, the 75 ns scheme

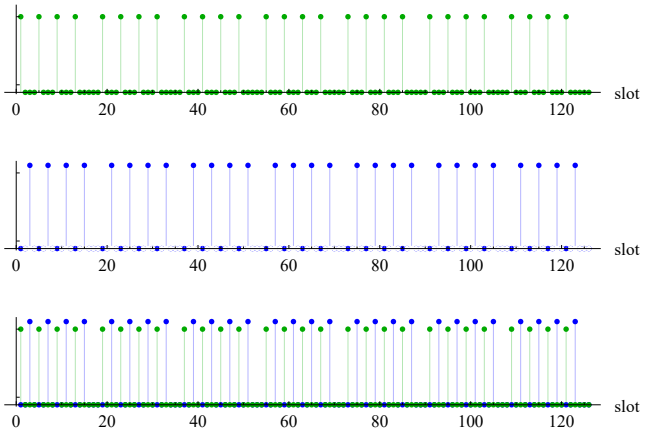

Figure 1: Schematic illustration of slip stacking of two 100/150 ns trains (blue and green) in the SPS to form a 50/100 ns train for injection into the LHC. The first number refers to the spacing between bunches within a PS batch, while the second number refers to the spacing between PS batches in the SPS.

used in 2018 remains available as a backup. The integrated luminosity would be 20-30% lower than with the 50 ns scheme, as shown in detail in Sec. 4.2.

2.2 Filling schemes

The details of the Pb filling scheme from 2018 are shown in the last row of Table 3. It relied on batches of 3 bunches with 75 ns created in LEIR and PS, and the sequential injection of such batches, spaced by 150 ns, in the SPS. The filling scheme finally deployed in the LHC contained a total of 733 bunches.

The future 50 ns scheme relies on injecting 2 bunches from LEIR to PS, where they are split into 4, spaced by 100 ns. Several such PS batches should then be injected sequentially in the SPS to form trains within which each 100 ns PS batch is spaced by 150 ns, the SPS injection kicker rise time, from the next, as depicted in the top plot of Fig. 1. The 50 ns filling schemes to be presented below feature 7 or fewer PS batches at this stage for reasons given in [19].

Two such trains can then be interleaved using slip-stacking in the SPS to form a train spaced mainly by 50 ns except for spacings of 100 ns between sub-trains of 8 bunches as shown in [19] and in Fig. 1. The final train contains bunches from 14 PS batches. Shorter trains containing $8n$ bunches for $1 < n < 7$ are also useful in optimising the LHC filling schemes.

Two 50 ns filling schemes were presented in 2017 [17] with 1232 bunches in the LHC. We call them 1232b_1232_1168_0 and 1232b_1136_1120_81, defined with the customary naming convention indicating the total number of bunches

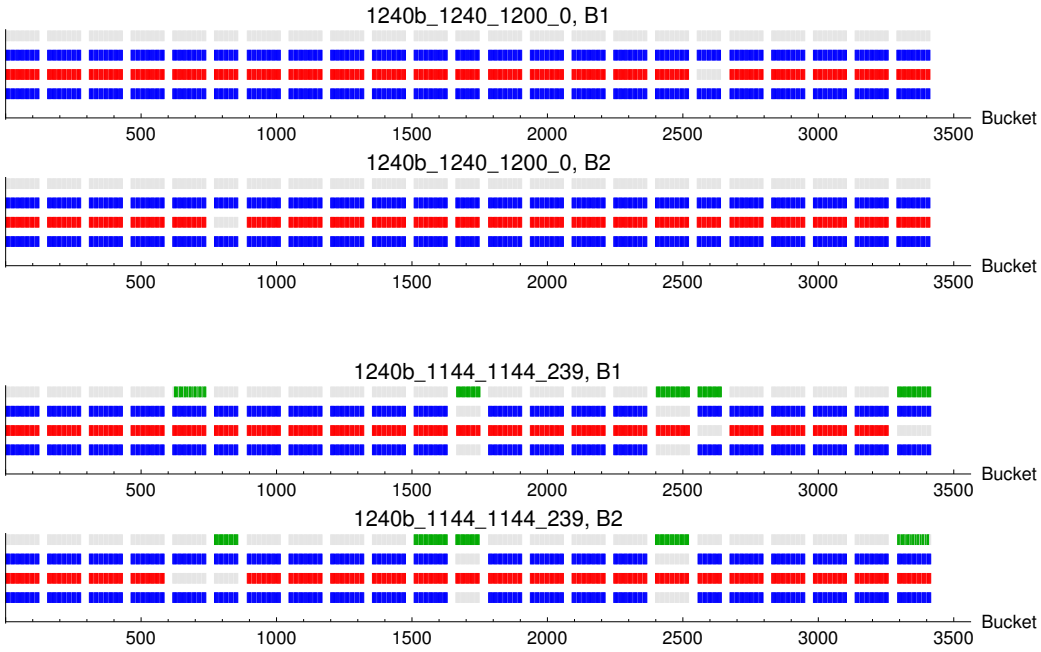

Figure 2: Illustration of the encounters experienced by each beam in the filling schemes 1240b_1240_1200_0 (top two plots) and 1240b_1144_1144_239 (bottom two plots). Each box represents a train, which is grayed out if it does not collide and is coloured if it collides. The top row in each figure represents collisions at IP8 (green for the colliding bunches), the second and fourth row collisions at IP5 and IP1 (blue), and the third row collisions at IP2 (red).

(b) followed by the number of collisions at ATLAS/CMS, ALICE, and LHCb, respectively. The first scheme had bunch encounters only in ALICE, ATLAS and CMS, and the second provided 81 encounters in LHCb.

Since then, LHCb has requested a significantly higher integrated luminosity, targeting 2 nb^{-1} until the end of Run 4 [18]. Therefore, new Pb filling schemes with 1240 bunches have been devised. We assume for all schemes a 150 ns rise time of the SPS injection kicker for Pb ions and a 800 ns rise time of the LHC injection kicker. The LHC abort gap keeper (AGK), which prevents injections into the abort gap, has been adjusted so that injections beyond RF bucket 33201 are forbidden. This value is slightly larger than the previous one, giving a little more flexibility and allows 1240 bunches instead of 1232[1].

With the new AGK value, the simplest scheme without collisions in LHCb, based on approximate quadrant symmetry, is 1240b_1240_1200_0, illustrated in

[1]Note that if the maximum number of PS injections into an SPS train is increased beyond 7, the AGK will have to be reduced, and conversely.

the top part of Fig. 2. Another new scheme, 1240b_1144_1144_239, is shown below it. The latter scheme was found by adjusting the spacings between, and the lengths of, the LHC trains. It provides slightly more bunch encounters at IP1/2/5 compared to the previous baseline 1232b_1136_1120_81, but almost a factor 3 more encounters at IP8.

Five new schemes are presented in Table 3, providing a range of different number of collisions at LHCb, while maintaining similar numbers at ATLAS, ALICE, and CMS. In the last scheme, more than 700 collisions are achieved at LHCb, and almost 1000 at the other experiments. Detailed injection specifications for each filling scheme are given in Appendix A.

Because of the ring symmetry and the displacement of the LHCb interaction point by 15 RF buckets (i.e. 37.5 ns) away from the symmetry point at 7/8th of the LHC circumference, collisions in LHCb require trains to be displaced longitudinally away from a perfect quadrant symmetry.[2] In general, this comes at the expense of decreased number of collisions at the other experiments. In the new filling schemes, the penalty for the other experiments could be kept moderate, but it is not negligible. The predicted performance with each scheme is discussed in Sec. 4.[3] The final filling scheme has to be selected giving appropriate weight to the requirements of the experiments. As has been done in the past, switching from one scheme to another during a run will be possible, to adjust final integrated luminosity outcomes. Other filling schemes could also be investigated in the future.

For p-Pb operation, we have not yet studied detailed filling schemes for the proton beam, which remains as future work, and we assume the same filling schemes as for Pb-Pb. In Sec. 4.4, a small margin is subtracted from the estimated luminosity to compensate for the fact that it might not be possible to construct identical schemes for protons. Indeed, this was the case in the last p-Pb run in 2016.

2.3 LHC beam parameters in collision

The LHC beams are expected to suffer from some degradation between injection and collision, as inevitable losses and emittance blowup occur. Losses before the beams go in collision are caused by, e.g. imperfect capture at the start of the energy ramp, dynamic aperture, diffusion, and residual gas scattering, while intra-

[2]The "naturally-constructed", approximately quadrant-symmetric, 100 ns and 50 ns filling schemes originally envisaged for heavy-ion operation did not provide any collisions at LHCb (as none were required). This is not the case for the 25 ns schemes used in proton operation.

[3]As Fig. 2 shows, different bunches experience different numbers of collisions, at IPs with potentially different values of β^* and will therefore have different lifetimes. So the integrated luminosity is not simply proportional to the number of collisions and β^* at each IP.

Filling scheme	no. of bunches	no. of collisions at IP1/5	IP2	IP8	spacing
1240b_1240_1200_0	1240	1240	1200	0	50 ns
1240b_1144_1144_239	1240	1144	1144	239	50 ns
1240b_1088_1088_398	1240	1088	1088	398	50 ns
1240b_1032_1032_557	1240	1032	1032	557	50 ns
1240b_976_976_716	1240	976	976	716	50 ns
733b_733_702_468	733	733	702	468	75 ns

Table 3: Possible filling scheme for heavy-ion operation in Run 3 and Run 4, defined with a naming convention indicating the total number of bunches (b) followed by the number of collisions at ATLAS/CMS, ALICE, and LHCb respectively. The 733b_733_702_468 scheme was already used operationally in 2018 and is retained as a backup in case the 50 ns beams, depending on SPS slip-stacking, are not available.

beam scattering (IBS) is the main source of emittance blowup. It is partly or fully compensated by emittance shrinkage due to synchrotron radiation damping [1, 21].

For the 2018 scheme with 75 ns, we list the achieved beam parameters at the start of collisions in Table 4. The numbers shown refer to the average over all 75 ns physics fills in 2018, where an intensity loss of 6–7% was observed between injection and the start of physics. It should be noted that the emittance was measured using the synchrotron light monitor (BSRT), which was not calibrated in detail for Pb beams. However, as shown in Sec. 4, the measured luminosity matches well the one calculated using the BSRT measurement, meaning that the missing BSRT calibration should not introduce a significant error. The values shown are the average over the two beams and planes, where the horizontal emittance is typically a bit larger (around 2.4–2.6 μm) and the vertical emittance is a bit smaller (around 2.1–2.3 μm).

For the future HL-LHC at 50 ns, we assume a similar change in beam properties as observed in the past [17]. An emittance blowup of about 10% between injection and flat top has been estimated, as well as a 5–7% intensity loss. This provides an estimate of the beam parameters at the start of Stable Beams, shown in Table 4. The performance estimates in Sec. 4 are based on these values.

For p-Pb operation, we assume the same Pb beam as in Table 4. The proton beam is assumed to have normalized emittances around 2.5 μm as for p-p operation, with intensities *chosen* to be 3×10^{10} protons per bunch. This is slightly larger than the maximum used in 2016. Larger proton intensities make little sense when ALICE is levelled, since they accelerate the degradation of the Pb beam as a result

	LHC design	2018	HL-LHC
Beam energy (Z TeV)	7	6.37	7
Bunch spacing (ns)	100	75	50
Total no. of bunches	592	733	1240
Bunch intensity (10^7 Pb ions)	7	21	18
Normalized transverse emittance (μm)	1.50	2.33	1.65

Table 4: Pb beam parameters at the start of collisions in LHC design report [1], as achieved in 2018 [7, 6], and as envisaged for HL-LHC [17]. The 2018 parameters are a typical average in the 75 ns fills.

of the fast luminosity burn-off in ATLAS and CMS. The resulting short beam lifetime and fill duration would be unfavourable for ALICE. It could be investigated though if a running scenario can be found with larger proton bunch intensities, and also ATLAS and CMS levelled, which could provide more luminosity for all experiments.

3 HL-LHC machine configuration

3.1 Beam optics and IP parameters

For HL-LHC Pb-Pb and p-Pb operation, a different optics has to be used than for proton operation. It is envisaged to squeeze ALICE, ATLAS, and CMS to $\beta^* = 0.5\,\mathrm{m}$ and LHCb to $\beta^* = 1.5\,\mathrm{m}$. At that β^*, it is not necessary to deploy the achromatic telescopic squeeze (ATS) [22], as envisaged for protons [13][4] . The integrated heavy-ion luminosity is not so sensitive to β^*, since the burnoff is anyway very fast due to the very high cross section, as opposed to proton operation, where a squeeze to $\beta^* = 0.15\,\mathrm{m}$ is foreseen at ATLAS and CMS. Therefore, the gain from squeezing to very small β^* is smaller with heavy ions than with protons. Nevertheless, some gain in integrated luminosity is possible also for heavy ions, as discussed in Sec. 4.3.

A heavy-ion optics with the foreseen β^*-values was already used in the 2018 Pb-Pb run [6, 23], and this optics is hence already rather close to the nominal goal for HL-LHC. However, the optics has to be rematched in the upgraded HL-LHC lattice, due to the new layout in IR1 and IR5, and it should be reachable through a seamless transition from the proton injection optics.

For protons, the HL-LHC baseline running scenario includes a levelling of the luminosity in ATLAS and CMS, in order to avoid a too high event pileup,

[4] Unless the ATS for protons is used to enhance Landau damping at larger β^* before collision and one needs to re-use the proton cycle to reduce commissioning time

through a dynamic change of β^* from 0.6 m to 0.15 m while keeping the beams colliding [13, 24]. This is necessary in order to avoid operating at the smallest β^* with the highest intensity, as the levelling with parallel separation reduces margins of beam stability. For heavy-ion operation, this is not a concern, and the baseline is instead to level the luminosity by varying the parallel separation at the IP. This has the advantage of allowing for a much simplified and faster commissioning and validation. This was demonstrated in the 2018 run with bunches spaced by 75 ns of higher intensity. A detailed tracking study for the HL-LHC baseline, with 50 ns spacing but lower bunch charge, is pending, but no issues are expected.

Because of the smaller bunch charge, larger bunch spacing, and larger β^*, the reduction of dynamic aperture due to the long-range beam-beam interactions is much less critical for heavy ions than for protons. Therefore, a significantly smaller crossing angle can be used. During Runs 1–2, the crossing angles were in the vertical plane in ALICE and ATLAS and horizontal in CMS and LHCb, following the scheme used for protons in which the relatively large beam-beam tune-spreads induced by the crossings in ATLAS and CMS are arranged to cancel to a large extent. Again, these beam-beam effects are relatively unimportant in heavy-ion operation and the option of, say, switching to a vertical crossing angle in CMS could be considered (this could resolve difficulties with the narrower ZDC detectors that will be installed for Run 4).

In 2018, the external half-crossing angle in ALICE was 137 μrad, which gave a net crossing angle of 60 μrad at the IP after subtracting the 77 μrad angle induced by the spectrometer compensation bump [6]. For HL-LHC, the bunch spacing will be 50 ns and a 170 μrad half external crossing angle is assumed [17], which corresponds to a normalised beam-beam separation of 10.2σ at $\beta^* = 0.5$ m at 7 Z TeV and a 6σ separation at the closest encounter [25]. With the 70 μrad spectrometer angle subtracted, this results in a 100 μrad net half-crossing angle at ALICE. However, if the net angle goes above 60 μrad in the present LHC, the spectator neutrons emerging from the collisions are collimated to an unacceptable degree before they reach the Zero Degree Calorimeter (ZDC), located about 114 m from the IP. An upgrade is therefore being implemented in LS2 to increase the aperture of one collimator and move it slightly in order to reduce this effect to an acceptable level [26], even with a half-crossing angle of 100 μrad.

It should be noted that ALICE usually switches the polarity of the spectrometer at the mid-point of each run. At the same time, the polarity of the external crossing angle is changed, so that the net crossing angle simply changes sign.

At ATLAS and CMS, there are no limiting aperture constraints for the envisaged β^*. It is foreseen to use a half crossing angle of 170 μrad, corresponding to the external angle used in ALICE. At LHCb, we assume also an external half crossing angle of -170 μrad. The spectrometer angle of -135 μrad has to be added to this, yielding a net half angle of -305 μrad. Since the crossing plane is

	IP1	IP2	IP5	IP8
β^* (m)	0.5	0.5	0.5	1.5
crossing plane	V	V	H	H
spectrometer half crossing (μrad)	0	$\mp$70	0	-135
external half crossing (μrad)	170	$\pm$170	170	-170
net half crossing (μrad)	170	$\pm$100	170	-305
spectrometer polarity	-	pos/neg	-	pos

Table 5: Baseline parameters at the HL-LHC IPs in collision for Pb-Pb operation at $7Z$ TeV.

horizontal, the external angle must be negative in order to add to the beam-beam separation given by the D1/D2 separation dipoles and not introduce parasitic encounters. With positive spectrometer polarity, the internal angle is negative, so that it adds to a negative external angle. With negative spectrometer polarity, when internal and external angles compensate, the external angle must be larger in absolute value to keep the net angle negative. The LHCb polarity was positive in the 2018 Pb-Pb run, and we assume here that this will be the case also for future Pb-Pb runs. With negative polarity, a smaller net angle could be envisaged. Using, say, an external half angle of $-235\,\mu$rad, a net angle of $-100\,\mu$rad could be obtained, as in ALICE.

The main parameters at the IPs for Pb-Pb operation in collision, as discussed above, are summarized in Table 5.

The same optics and crossing angles as in Pb-Pb are assumed for p-Pb.

3.2 Collimation and aperture protection

The LHC and HL-LHC feature a multi-stage collimation system [1, 27, 28, 29], which should clean the unavoidable halo, localize losses, provide passive machine protection [30, 31], and reduce experimental backgrounds [32, 33] for both protons and heavy ions. It features betatron cleaning in IR7 and momentum cleaning in IR3. The movable collimators have to protect the aperture sufficiently throughout the HL-LHC cycle, and their settings for Pb-Pb operation are summarized in Table 6. The same settings are assumed for Pb-Pb and p-Pb operation, with the exception of the physics debris absorbers (TCLs) as mentioned below.

The stages of the collimation hierarchy will remain the same as in Run 2, although some of the collimators will be upgraded with a new low-impedance design [13]. Therefore, the settings in units of beam σ are also almost identical to the ones successfully used in the 2018 Pb-Pb run [34]. Otherwise, a major difference is the addition of the dispersion suppressor collimators (TCLDs) in

Function	name	IR	Setting at injection (σ)	Setting at flat top (σ)	Setting at collision (σ)
Primary collimator	TCP	7	6.7	5.9	5.9
Secondary collimator	TCS	7	7.9	7.7	7.7
Active absorber	TCLA	7	11.8	11.8	11.8
DS collimator	TCLD	7	out	16.6	16.6
Primary collimator	TCP3	3	9.5	17.7	17.7
Secondary collimator	TCS	3	11.0	21.3	21.3
Active absorber	TCLA	3	14.2	23.7	23.7
Tertiary collimator	TCT	1/5	15.4	17.7	10.6
Tertiary collimator	TCT	2	15.4	17.7	10.6
Tertiary collimator	TCT	8	15.4	17.7	17.7
DS collimator	TCLD	2	out	out	47.3
Dump protection	TCDQ	6	9.5	8.6	8.6
Dump protection	TCSP	6	8.9	8.6	8.6

Table 6: Collimator settings at injection, at the flat top energy of $7Z$ TeV, and in physics operation with Pb beams. All settings are given in units of beam σ, for a normalized reference emittance of $1.0\,\mu$m, chosen to give a geometric emittance equivalent to a normalized proton emittance of $2.5\,\mu$m as usually used for HL-LHC collimator settings. The settings expressed in σ using the LHC equivalent proton emittance, as well as the real ion emittance, are shown for comparison in Appendix B. Most settings are identical in mm to what was used operationally in 2018 [34]. For IR1 and IR5 in Run 4, when the new large-aperture HL-LHC triplets will be available, the TCT settings could potentially be relaxed. In the case of the TCLDs in IR2, the setting quoted corresponds to a 5 mm hafgap.

IR2 and IR7 to cope with the increased Pb beam intensity and luminosity.

The smallest aperture that can be protected by the collimation hierarchy[5] in Table 6 is 11.8σ, although there is machine-protection margin to tighten the hierarchy additionally as was done for protons in 2018[6] [35]. However, with a tighter hierarchy, the risk of significant losses on the tertiary collimators (TCTs) increases, which could cause both higher experimental backgrounds and premature beam dumps during any loss spikes. This option could be further studied, but the baseline is to keep the 10.6σ TCT setting, which could even be increased if the

[5]This assumes a normalized emittance of $1.0\,\mu$m, equivalent to $2.5\,\mu$m for protons at the same magnetic rigidity. The same emittance value is used for all aperture estimates in this section.

[6]Thanks to a favourable phase advance between the extraction kickers and sensitive equipment, which minimizes the risk of damage during an erroneous trigger of the kickers, the protected aperture could be reduced to 8.8σ, which allowed $\beta^* = 0.25$ m in IR1 and IR5 for proton operation.

available triplet aperture is sufficient, as done operationally in IR1 in 2018 [34]. For IR1 and IR5 in Run 4, when the new large-aperture HL-LHC triplets will be available, the TCT settings could be relaxed significantly.

The global aperture was measured with Pb beams in the 2018 physics configuration ($\beta^* = 0.5\,\mathrm{m}$, half external crossing angle of $137\,\mu\mathrm{rad}$ in ALICE and $160\,\mu\mathrm{rad}$ in ATLAS and CMS), for both polarities of the ALICE crossing angle, and for both beams and planes [36, 37]. The results[2] show that all apertures were at least 0.7σ above the required 11.8σ, and the smallest IR2 bottleneck was at 15σ. This measurement was done with the ALICE IP displaced vertically by $-2\,\mathrm{mm}$ through an additional bump. The ALICE detector will be realigned in LS2 to dispense with the need for this bump in Run 3 and thereby improve the aperture. Therefore the available aperture in the baseline configuration is expected to be adequate.

In terms of halo cleaning, the achieved efficiency in Run 2 is about two orders of magnitude worse for Pb ions than for protons, because of ion fragments with an altered magnetic rigidity created in the primary collimators (TCPs) [38, 39, 40, 41]. The criticality of these losses was shown in a 2015 test where a magnet quenched [42]. This makes collimation more critical for Pb than for protons in HL-LHC, although the 20 MJ stored energy of a Pb beam energy is by far less than the 700 MJ of the proton beam. To improve the cleaning performance, one new collimator per beam (called TCLD) is scheduled for installation during LS2 on the downstream side of the dispersion suppressors (DS) in IR7. To make space for the TCLD, a standard 8 T dipole magnet will be removed and replaced by two shorter and stronger 11 T magnets, with the TCLD in between [13].

The Pb cleaning performance of the upgraded HL-LHC collimation system has been assessed with simulations using the SixTrack-FLUKA coupling [41]. A simulated loss distribution around the ring is shown in Figs. 3. The main losses occur on IR7 collimators and all cold locations are well protected thanks to the TCLD, which almost completely cleans the particles that would otherwise be lost around the ring. The only significant cold losses are in the IR7 DS, on the 11 T magnet upstream of the TCLD. The energy deposition studies in [43] show that these losses are well below the quench level for design losses.

For the proton beam in p-Pb operation, the cleaning is not critical, since the intensity used is much lower than during the standard proton runs.

In addition to the system presented in Table 6, crystal collimation [44] has recently been integrated into the HL-LHC baseline. It is being pursued to cure the DS losses with Pb beams in case of schedule risk for the 11 T magnets and to provide further cleaning improvements if needed. In this scheme, the halo particles impact first on a bent silicon crystal, where they travel between the crystal planes with a much reduced probability of nuclear interactions. The bending of the crystal can coherently deflect the beam halo onto a downstream absorber. Very

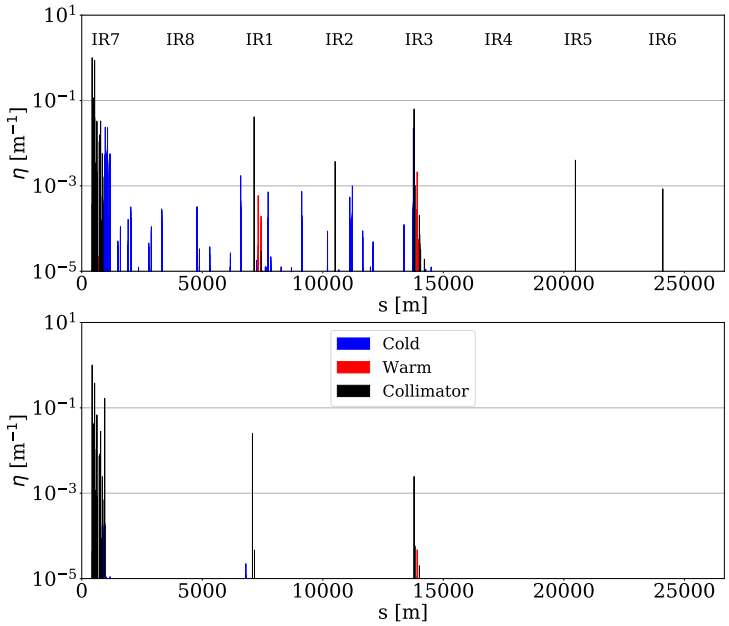

Figure 3: Simulated loss pattern around the ring for the LHC 2018 configuration without TCLDs (top) and HL-LHC including the TCLD (bottom). A horizontal halo in B1 was considered.

promising results were obtained in Run 2 using an LHC test installation [45, 46] but some further development and upgrades are needed, especially on controls, to ready the system for operation [13].

3.3 Alleviation of collisional losses

3.3.1 Pb-Pb OPERATION

Had it not been levelled, the peak luminosity at the ALICE experiment would already have been limited by local losses from secondary beams created by ultra-peripheral nuclear interactions between the colliding Pb beams at the IP [47, 48, 49, 50, 51, 52]. The most important process is bound-free pair production (BFPP) [53, 54], in which one of the colliding Pb^{82+} ions acquires an extra electron. The resulting Pb^{81+} ions, with a changed charge-to-mass ratio, are lost in a localized spot in the DS, where the dispersion generated locally since the IP has risen significantly. These losses would lead to a quench of the impacted magnet at high enough luminosity, as shown experimentally in 2015 [55, 56].

In HL-LHC, the BFPP beam carries about 180 W of power for a luminosity of 7×10^{27} cm^{-2}s^{-1}. Further localized losses are caused by 1- or 2-neutron electromagnetic dissociation (EMD1 and EMD2) where one nucleus emits one or two neutrons, thus changing mass [53, 57]. Other photon-induced processes also take place, but these cross-sections are dominant.

In IR1 and IR5, the BFPP beam is lost in the last dipole in cell 11, close to an empty connection cryostat. Therefore, the risk of quenches can be mitigated by redirecting the losses from the magnet to the empty cryostat using a local orbit bump [56]. Such bumps have been routinely used in the 2015 [4] and 2018 [6] Pb-Pb runs. In the 2018 run, a peak luminosity of 6.1×10^{27} cm^{-2}s^{-1}, close to the HL-LHC target, was reached in IP1 and IP5. Simulation studies also confirm that, at a luminosity of 7×10^{27} cm^{-2}s^{-1} and at a beam energy of 7 Z TeV, the power deposition in the nearby superconductors (including bus bars and magnets) would remain safely below the quench level with a significant margin [58], making the orbit bumps a robust solution.

This technique does not work in IR2, where the BFPP beam is lost upstream of the empty cryostat, because the quadrupoles have opposite polarities with respect to IR1 and 5. Bumps were nevertheless used in IR2 to spread out the losses, as discussed in [51], but the gain in energy deposition on magnets is much smaller than if the beam can be steered into the empty cryostat. This small gain is not enough to reach the HL-LHC design goal. Instead, a TCLD collimator is being installed during LS2, in the connection cryostat in cell 11 on each side of IP2. In this case there is no need for 11 T magnets to free space. An orbit bump is still required to pull the BFPP beam away from the aperture in cell 10 around $s \simeq 380$ m and make it hit the TCLD instead. The EMD1 beam, which carries about 65 W at a luminosity of 7×10^{27} cm^{-2}s^{-1}, can be intercepted with the other jaw. The envelopes of the main and secondary beams in IR2 are shown in Fig. 4 together with the TCLD in the final configuration, including the bump. Energy deposition studies predict that this solution will protect all nearby superconductors with a factor 10 of margin even at a luminosity of 7×10^{27} cm^{-2}s^{-1} [58, 59].

Table 7 summarizes the bump amplitudes used in IP1, 2 and 5 in 2015 and 2018.

In IR8, the quadrupole polarities are similar to those in IR2 and orbit bumps alone cannot be used to steer BFPP and EMD beams into the connection cryostat. No TCLD installation is presently foreseen. Since the local geometry and the impact distribution are different from IR5, we cannot directly assume the same power deposition and the luminosity limit found experimentally in [55]. We therefore conservatively assume that LHCb has to be levelled at 1×10^{27} cm^{-2}s^{-1} to stay safely below the quench level. This was demonstrated experimentally in 2018 [6]. Future studies could be performed to establish whether a higher luminosity could be tolerated.

	2015		2018	
IP	Left	Right	Left	Right
IP1	-3.2	-2.75	-2.6	-2.6
IP2	-3.0	-3.0	-2.6	-2.0
IP5	-3.0	-2.6	-1.6	-2.5
IP8	0.0	0.0	0.0	0.0

Table 7: BFPP bump amplitudes in mm used in Run 2. The value corresponds to the peak at the MQ11 for IR1 and IR5 and the peak at MQ10 for IR2.

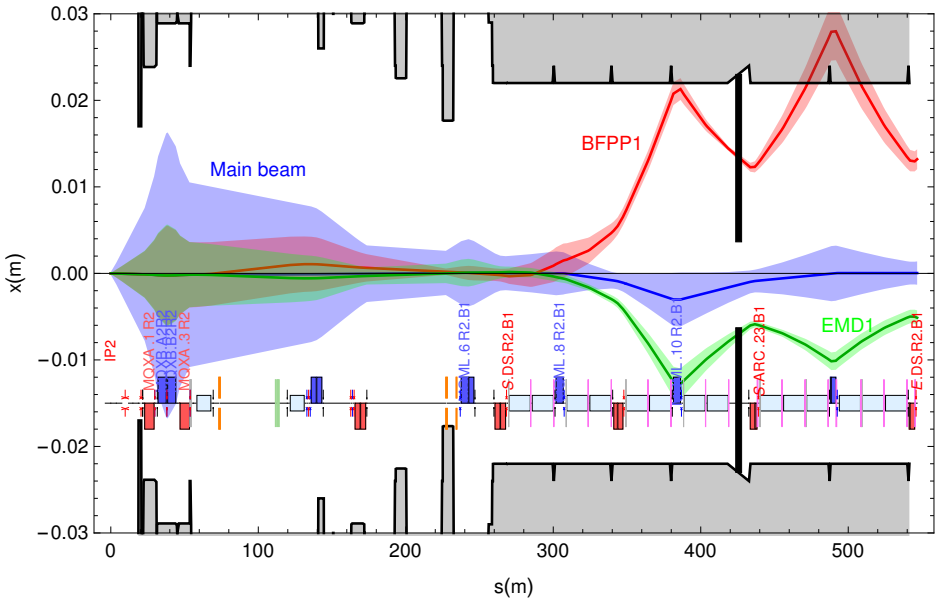

Figure 4: Envelope of the main $^{208}Pb^{82+}$beam (blue) together with the dispersive trajectories of ions undergoing BFPP1 (red) and EMD1 (green), coming out of the ALICE experiment (IP2). A closed orbit bump is in place, making the BFPP1 beam miss the aperture at $s \approx 380\ m$ and instead hit the TCLD collimator, shown as black lines at $s = 426$ m with an effective 47.3σ opening.

Even with the upgraded luminosities, the luminosity debris from the nuclear collisions in Pb-Pb operation carries a total power 30 times less than the BFPP beam and poses no risk of quenches.

3.3.2 p-Pb OPERATION

The cross-sections of the electromagnetic processes described above are much smaller in p-Pb operation. On the contrary, the luminosity debris from the Pb

beam is much higher and limited luminosity at the end of the 2016 run [11]. At a luminosity of 8.9×10^{29} cm^{-2}s^{-1} the signals on the beam loss monitors (BLMs) at the beginning of the dispersion suppressor right of IP1 reached about 90% of the dump threshold [60]. To reduce the risk of losing fills, the injected proton intensity was slightly decreased in the subsequent fills.

The luminosity in the HL-LHC could be about a factor 2.5 times higher, as shown in Sec. 4.4 and these losses therefore need to be limited. It has been shown [60] that the existing TCL collimators in IR1 and IR5, which were not used in 2016, could be used to intercept ion fragments which have a magnetic rigidity deviation of about 2% or more, while fragments with smaller deviations should be lost further downstream and not at the limiting location. It can be concluded that the target p-Pb luminosity should be within reach, although more refined quantitative estimate based on a realistic fragment distribution may be desirable.

In IR2 and IR8, there are no TCL collimators, but the foreseen luminosities are significantly lower. It is therefore unlikely that collisional losses there will limit the operation. The TCLD collimator in IR2 in combination with an orbit bump might help to intercept some fragments.

3.4 Beam stability

The LHC and HL-LHC impedance is dominated by the impedance of collimators, which are the devices closest to the beam. For Pb ions, the half-gaps of the largest impedance contributors, namely the collimators in IR3 and IR7, are very similar to that of protons at 7 TeV, so the impedance is very similar too [61].

The stability threshold I_{oct} in terms of octupole current is in general proportional to

$$I_{\mathrm{oct}} \propto \frac{N_b Z^2}{m_0 \gamma_{\mathrm{rel}}} \times \frac{1}{dQ_{\mathrm{oct}} \varepsilon_g}, \tag{1}$$

for N_b particles per bunch, each with rest mass m_0 (approximately proportional to A), with ε_g the geometric emittance and dQ_{oct} the detuning coefficient (w.r.t. to the action) per Ampere in the octupoles. Since $\varepsilon_g = \varepsilon_n/(\beta_{\mathrm{rel}}\gamma_{\mathrm{rel}})$, with ε_n the normalized emittance, and dQ_{oct} is the same for ions and protons at top energy, the dependency on γ_{rel} cancels out and one is left with a scaling by $N_b Z^2/(A\varepsilon_n)$, with $Z^2/A \simeq 32.6$ here. At constant magnetic rigidity, this scaling can also be expressed as the ratio of bunch charge to geometric emittance. In the end, the octupole threshold for HL-LHC Pb beams (see Table 14 in Appendix C) is around 7% of that needed for 10^{11} protons with $\varepsilon_n = 2\,\mu$m (with the same bunch length and number of bunches for Pb ions and protons, and at iso-impedance).

Assuming the HL-LHC beam parameters, the LS2 collimator impedance upgrade and no transverse damper, as a worst case scenario, we can calculate the octupole current necessary to stabilize a single beam, thanks to the DELPHI Vlasov

solver [62] combined with the stability diagram theory assuming a parabolic distribution [63], which is characterised by the absence of tails above 3.2σ (case of HL-LHC with an electron-lens, which is a pessimistic assumption, since it still needs to be investigated whether the hollow electron lens needs to be used during ion runs). Octupole thresholds vs. chromaticity are shown in Fig. 5, where we can see that for $10 < Q' < 20$, an octupole current of 30 A (with negative polarity) is enough to stabilize the beam (it would be around 25 A with positive polarity [61]). With the transverse damper on, with its gain set as low as $0.001/\text{turn}$, the threshold decreases to less than 14 A [61]. There is therefore a margin of more than an order of magnitude before the maximum octupole current is reached, even including the current discrepancy factor 2 between model and LHC measurements [64], or possible effects of long-range beam beam interactions.

We therefore conclude that the available octupole current should be ample to stabilise the Pb beams in HL-LHC. It should be noted, however, that the impedance of crystal collimators is not included in the impedance model; its evaluation is pending [65]. This is not expected to be limiting, since crystals were inserted without detrimental effects with a full machine during tests in the 2018 Pb run.

3.5 Longitudinal parameters

The RF voltage and longitudinal parameters used in the 2018 Pb-Pb run were presented in [66]. At injection, an RF voltage of 8 MV was used, which was increased to 12 MV at flat top, where typically a 1.1 ns, 4σ-equivalent bunch length[7] was achieved. In 2018, the bunch length after injection and adaptation to the LHC bucket was typically around 1.2 ns, equivalent to an emittance of 0.54 eVs with an RMS energy spread of 3.30×10^{-4}. At the start of the ramp, the average bunch length could reach up to 1.5–1.6 ns, equivalent to an emittance of 0.79–0.87 eV s with an RMS energy spread of $(3.90\text{–}4.07)\times10^{-4}$.

For HL-LHC, relying on slip-stacking in the SPS, the longitudinal parameters of the bunches injected in the LHC will be different. In particular, the longitudinal emittance is predicted to increase by about a factor 3, which will mainly be seen in the energy spread. Furthermore, the longitudinal bunch profiles will become somewhat hollow close to the bunch centre.

The optimal RF voltage and resulting bunch parameters at flat bottom in the LHC under the influence of IBS remain to be studied in detail. However, studies of the bunch evolution in the SPS under slip-stacking and the capture at the LHC give first estimates of the bunch parameters and indicate that 8 MV can still be

[7]The 4σ-equivalent bunch length is computed from the full-width-half-maximum measurement FWHM assuming a Gaussian distribution as $2/(\sqrt{2\ln 2})\text{FWHM}$.

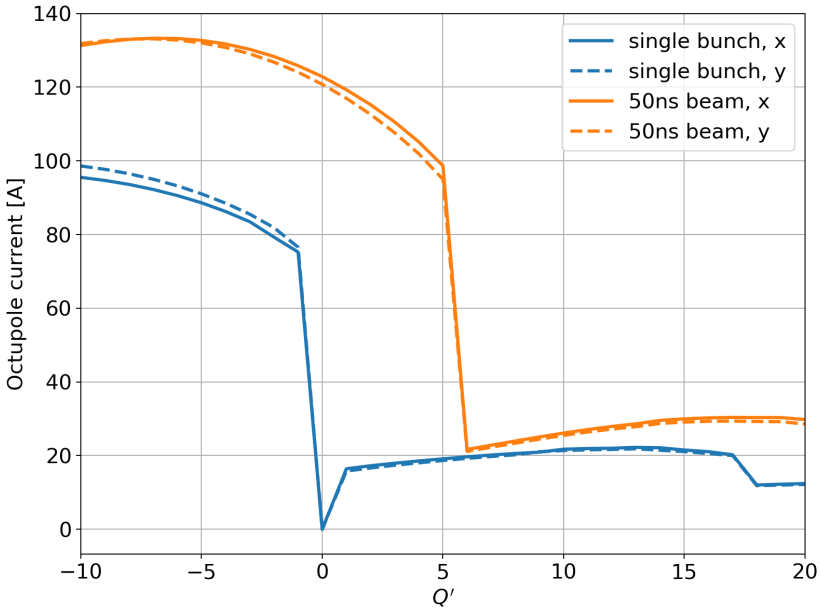

Figure 5: Octupole threshold vs. chromaticity for lead ions at flat top, with negative octupole polarity, no transverse damper, and for a parabolic transverse distribution. The LS2 collimator upgrade and HL-LHC parameters (Table 14 in Appendix C) are assumed.

used as capture voltage. We assume these values, summarized in Table 8, pending further studies.

The controlled longitudinal emittance blowup in the ramp ensures reaching the desired bunch length on arrival at flat top. The RF voltage at flat top, and with it the longitudinal emittance, can then be tuned somewhat to adjust the subsequent bunch length evolution in physics in the presence of IBS and synchrotron radiation. For this work it is assumed that the RF voltage will be 14 MV, slightly higher than in 2018. This causes a slower IBS growth rate and therefore a smaller transverse emittance, potentially resulting in a higher luminosity. Furthermore, we assume the same 1.1 ns, 4σ bunch length as in 2018, which was proven to work well, even with bunch intensities higher than those foreseen for the future 50 ns schemes. The bunch length could possibly be optimised further, since on one hand shorter bunches result in a better geometric reduction factor, but on the other hand they also enhance IBS growth of the transverse emittance. It remains as future work to study the sensitivity of the integrated luminosity to the longitudinal parameters and to find an optimum. The proposed longitudinal parameters

	Injection	Flat top
RF voltage (MV)	8	14
Bucket area (eVs)	1.48	7.12
Bunch length, 4 σ (ns)	1.4	1.1
Bunch length, 1 σ (cm)	10.5	8.24
RMS energy spread (10^{-4})	4.4	1.02
Longitudinal emittance (eV s / charge)	0.76	2.42

Table 8: Longitudinal parameters for Pb beams foreseen at injection and flat top (assuming 7 Z TeV). The parameters at injection depend on bunch conditions as injected from the SPS after slip-stacking, while the flat-top conditions can be adjusted with the longitudinal blowup target during the energy ramp in the LHC.

are summarised in Table 8.

4 Projected heavy-ion performance in Runs 3 and 4

4.1 Simulation tools and benchmark

Using the configuration from previous sections, we can estimate the luminosity performance in typical Pb-Pb and p-Pb fills in HL-LHC. For this we use two independent simulation tools in order to increase confidence in the results. The first one is Collider Time Evolution (CTE) [21, 67, 52]. CTE tracks bunches of macro particles using a one-turn map, including sequentially the effects of collisions, betatron motion, longitudinal motion, intra-beam scattering (different models are available in the program—here we use the Nagaitsev model [68], without any added mixing between the horizontal and vertical growth rates), radiation damping, machine aperture, extra losses modelled through a non-collisional lifetime, emittance blowup from additional sources[8]. and luminosity levelling. The filling scheme can either be modelled through a fast and simplified approach, where the full beam is represented by one macro bunch and the collision probability (luminosity burn-off) at each IP is scaled by the number of real bunches colliding, or through a more detailed, but slower approach where one macro bunch is tracked per beam and per beam-beam equivalence class, as defined in [69], and realistic collisions between the bunches are simulated. For the CTE studies in this report, we rely on the approach with one macro bunch per beam, since it provides speed and simplicity in the setup and, as will be shown in the following, the results are in very good agreement with LHC data.

[8]Stochastic cooling can also be included, but was not used

The second simulation code, which we call the multi-bunch simulation (MBS), is based on a set of coupled differential equations for bunch intensities and beam phase space moments, including the effects of luminosity burn-off, IBS using the the so-called completely integrated modified Piwinski model [70, 71], radiation damping, and extra losses [60]. MBS models all bunches in the ring and the detailed collisions according to the real filling scheme, but relies on the assumption of Gaussian bunch distributions, as opposed to CTE where the tracked particles can assume any distribution. Extra losses can be added, which are specific to bunches colliding at a special IP. On the other hand, the change of the beam distribution caused by the burn-off, included by construction in CTE, is neglected. The two codes can be seen as complementary.

To compare the simulations with data, 30 out of the 46 physics fills in the 2018 LHC Pb-Pb run were simulated in detail with CTE. The remaining 16 fills were deselected due to either bad data quality, very short fill lengths, or non-standard operational conditions. For each fill, the starting conditions for the total intensity, average emittances, and target values for the luminosity levelling were taken from the logged data. In the first part of the run, where the ALICE beam size was not correct due to an error in the local coupling correction [72], an effective β^*-value of 0.9 m was assumed. This value, which reproduces well the measured luminosity in the simulated fills, is based on the luminosity scans in [73]. It is the β^* that would give the same emittance in the ALICE scans as the value inferred from the scans at ATLAS and CMS. From this starting point, the simulated beam parameters and luminosity evolve independently in the simulations and no further input from measurements was used. Since non-colliding bunches in the machine showed on average a 100 h lifetime, we applied the same non-collisional lifetime in the simulations but did not include any additional emittance blowup. A total cross section of 509 b for particle removal was assumed for the $6.37Z$ TeV fills, consisting of the contributions shown in Table 9.

A few typical results are shown in Fig. 6. For each fill, the simulated and measured evolution of the instantaneous and integrated luminosity can be seen, as well as the beam intensity, and an excellent agreement is found in these quantities. A fair agreement is found also in the emittance evolution. This comes in spite of an uncertainty on the measured emittances from the BSRT, which was never properly calibrated for Pb beams in the 2018 run[9]. Nevertheless, using the measured emittance values at the start of each fill results in a very good agreement in the key observables in Fig. 6, and it is therefore likely that the real error on the emittance measurement is small.

In practical terms, the most important quantity for the simulation benchmark

[9] We applied only a very rough scaling based on a few parasitic wire scans taken during the initial commissioning.

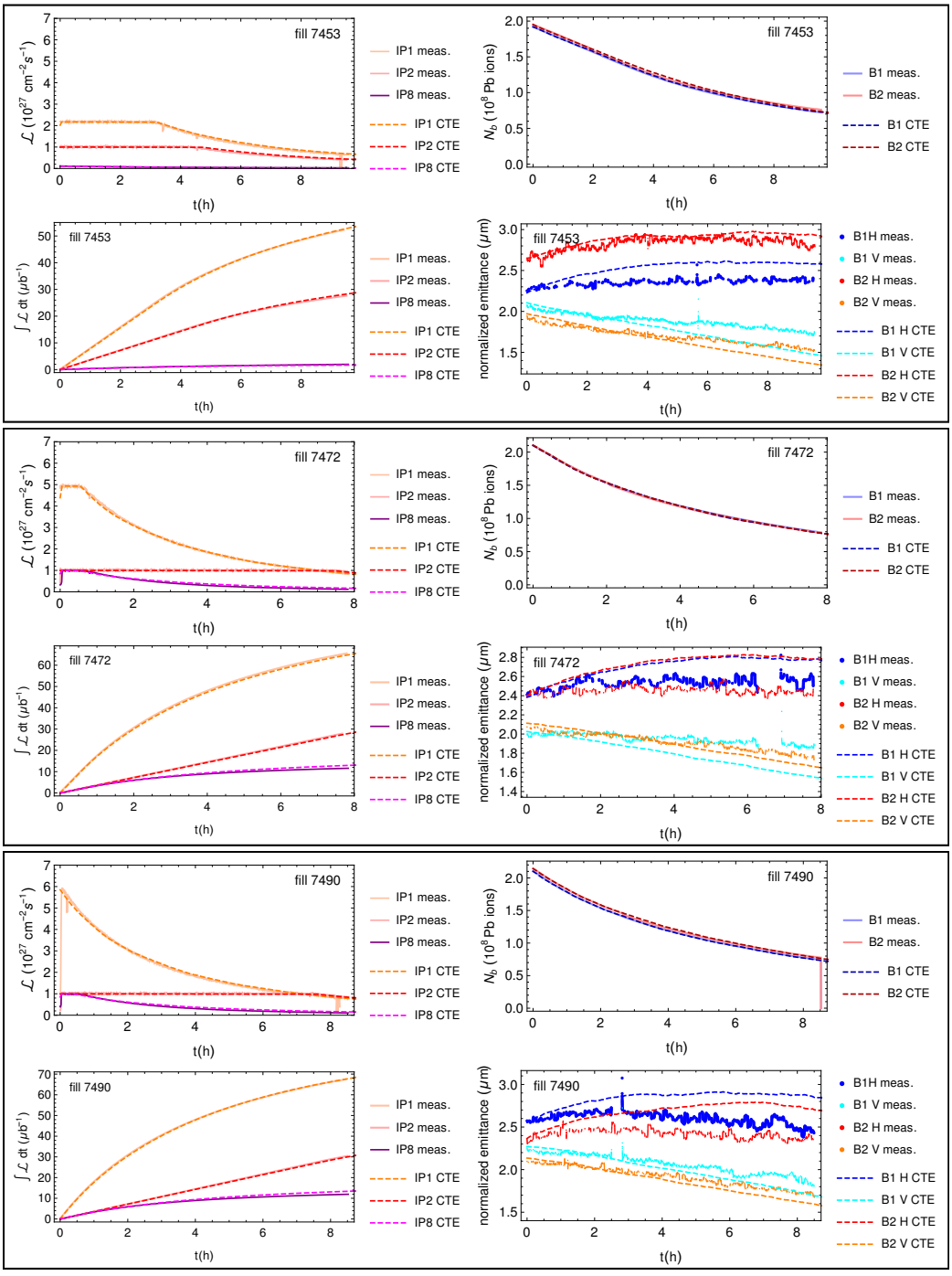

Figure 6: The measured evolution (solid lines) of key observables (instantaneous luminosity, integrated luminosity, average bunch intensity N_b, and average transverse emittances) during three typical Pb-Pb fills (7453–top, 7472–middle, 7490–bottom) from the 2018 LHC run, compared to CTE simulation results (dashed lines). The IP5 luminosity is not shown but is almost identical to the one in IP1.

	6.37ZTeV Pb-Pb	7ZTeV Pb-Pb	7ZTeV p-Pb
Hadronic inelastic (b)	7.7	7.8	2.13
BFPP (b)	278	281	0.044
EMD (b)	223	226	0.035
Total(b)	509	515	2.21

Table 9: Burn-off cross sections for various interactions between colliding Pb-Pb beams at 6.37ZTeV or 7ZTeV beam energy, and for 7Z TeV p-Pb collisions. The 7ZTeV Pb-Pb values are obtained from Refs. [1, 54, 74, 75, 76] and the 6.37ZTeV TeV ones are estimated using a scaling by the fixed-target frame γ of $\log(2\gamma^2 - 1)$. In accordance with Refs. [54, 76, 57], such a scaling is very close to the complete calculation. The p-Pb values are taken from [60]. The EMD cross sections include all decay channels.

is the integrated luminosity at the end of each fill. The ratios of that quantity between CTE and measurements in the 30 simulated fills are shown in Fig. 7. For the fills analysed, the average ratio of simulated and measured luminosity integral is 1.00 for ATLAS with a standard deviation of 0.03, and 1.01 for ALICE with a standard deviation of 0.04. At LHCb, the mean is 1.02, but the spread is much larger, with a standard deviation of 0.12. The detailed reason for this is not clear, although it might be related to uncertainties in the LHCb luminosity calibration [77]. Nevertheless, we consider the overall agreement very good.

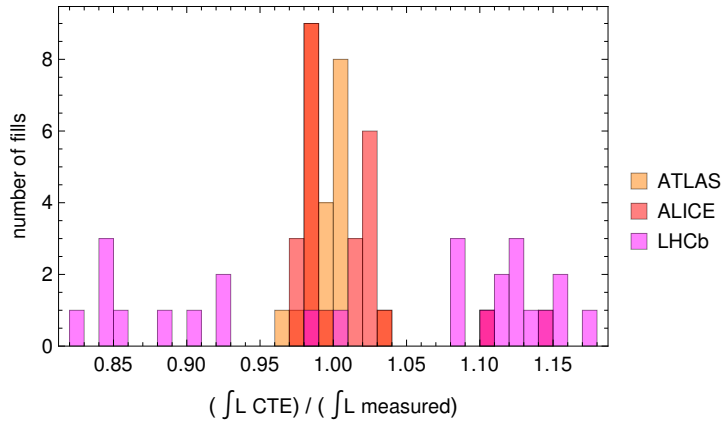

Figure 7: Distribution of the ratio of simulated to measured integrated luminosity for ATLAS, ALICE and LHCb per fill in the 2018 Pb-Pb run. CTE was used for the simulations.

MBS has been benchmarked with LHC p-Pb data in [60] and a detailed study is not shown here. In Fig. 8, MBS results are compared with CTE and LHC data

for one typical Pb-Pb fill from 2018, where a 100 h non-collisional lifetime was used in both codes. The agreement is very good, although a minor discrepancy is observed at the end of the ALICE levelling. These results confirm that both CTE and MBS can reliably predict the luminosity performance in future Pb-Pb and p-Pb operation.

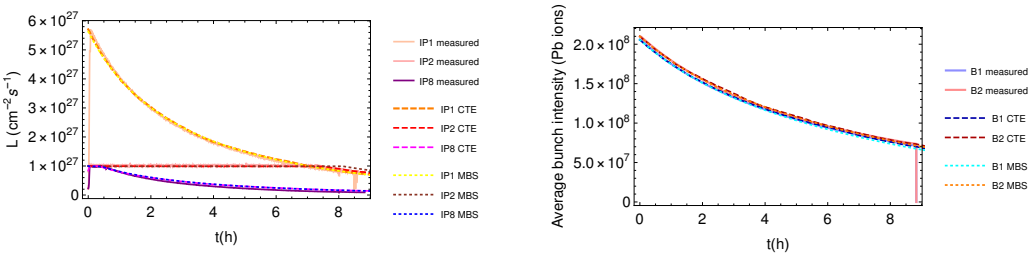

Figure 8: The evolution of key observables (instantaneous luminosity–left, average B1 and B2 bunch intensity–right) during one typical Pb-Pb fill (7477) at 6.37 Z TeV beam energy from the 2018 LHC run. Simulations from CTE and MBS are shown together with LHC data.

4.2 Pb-Pb performance in the HL-LHC baseline configuration

After LS2, the upgraded ALICE detector will accept a hadronic event rate of 50 kHz [14]. For a hadronic cross section of 7.8 b, this corresponds to a luminosity of 6.4×10^{27} cm^{-2}s^{-1}, which we assume as a levelling value in the simulations. We assume the same levelling at ATLAS and CMS for simplicity, although these experiments could potentially accept a higher luminosity. In IR8, we assume levelling at 1×10^{27} cm^{-2}s^{-1} to avoid quenches from BFPP.

The total cross section, for particle removal in the collisions at 7 Z TeV is given in Table 9. As can be seen, it is dominated by the electromagnetic processes, and the hadronic part is a minor contribution. Because of the very large total cross section, $\sigma_{\rm tot}$, the Pb ion operation is in a strong burn-off regime, where the total number of injected Pb ions, $N_{1,2}$ in either beam, determines the maximum possible integrated luminosity,

$$\sum_{\rm expts} \int_0^{T_{\rm f}} \mathcal{L}(t)\, dt \leq \frac{\min(N_1, N_2)}{\sigma_{\rm tot}} \tag{2}$$

where equality is approached in the limit of vanishing non-collisional losses and exhaustion of lesser beam as the fill length $T_{\rm f} \to \infty$. In typical heavy-ion fills the ratio of the two sides of this inequality, the *luminous efficiency*, exceeds 50–60%.

A typical fill with the machine configuration detailed in previous sections was simulated with CTE for the filling schemes in Table 3, using a 100 h non-collisional beam lifetime as in 2018. We use the beam parameters in Table 4 for the 50 ns and 75 ns schemes, except that we also use a $7Z$ TeV energy with the 75 ns beam. The resulting luminosity, intensity, and emittance evolutions are presented in Fig. 9. As can be seen, the intensities and emittances are similar between different 50 ns filling schemes, while different initial parameters are assumed for the 75 ns scheme. ATLAS, ALICE, and CMS are levelled in all 50 ns scenarios, with a levelling time up to about 2 h. ALICE has a slightly longer levelling time because of its smaller crossing angle. At LHCb, levelling is only needed for the three filling schemes with most collisions there. The luminosity at LHCb is lower than at the other experiments because of its lower levelling target, fewer colliding bunches, the larger β^*, and larger crossing angle. The integrated luminosity improves drastically in LHCb when the filling scheme is changed to have more collisions there, at the price of a moderate reduction for the other experiments.

As usual, the optimal fill length (time spent in collision), T_f, can be calculated to maximise the average luminosity $\mathcal{L}_\mathrm{avg}$

$$\mathcal{L}_\mathrm{avg}(T_\mathrm{f}) = \frac{\int_0^{T_\mathrm{f}} \mathcal{L}(t)\,dt}{T_\mathrm{f} + T_\mathrm{ta}}, \tag{3}$$

where $\mathcal{L}(t)$ is the instantaneous luminosity given by the simulation, and T_ta is the turnaround time, i.e., the time between the dump and the start of the collisions in the next fill. In reality, the turn-around time is the sum of a minimum irreducible value and a random value whose distribution reflects the general operational efficiency but cannot generally be predicted before the previous fill is dumped. However for the sake of simplicity and consistency with the corresponding treatment for protons [13, 24], we assume a typical value of $T_\mathrm{ta} = 200$ min, based on the detailed time estimates for all steps in [17].

As an example, $\mathcal{L}_\mathrm{avg}(T_\mathrm{f})$ is shown in Fig. 10 for ATLAS, ALICE, and LHCb, for the `1240b_1088_1088_398` scheme. It turns out that the optimum fill time, $T_\mathrm{f,opt}$, does not differ much between experiments. For the 50 ns schemes, it is around 3.8–3.9 h for ATLAS, 4.0–4.1 h for ALICE, and 3.6–4.5 h for LHCb. The spread in $T_\mathrm{f,opt}$ is largest at LHCb, but the curve of $\mathcal{L}_\mathrm{avg}$ is also very flat (see Fig. 10). Therefore, in the following, we can adopt the value of $T_\mathrm{f,opt}$ calculated for ALICE for each filling scheme.

The integrated luminosity $\mathcal{L}_\mathrm{tot}$ in one Pb-Pb run is then estimated as

$$\mathcal{L}_\mathrm{tot} = \mathcal{L}_\mathrm{avg}(T_\mathrm{f,opt}) \times T_\mathrm{run} \times \eta, \tag{4}$$

where T_run is the total time allocated to the physics run. Typically one month per year is allocated for heavy-ion operation, where the first week is used for commissioning. We assume thus $T_\mathrm{run} = 24$ days available for physics.

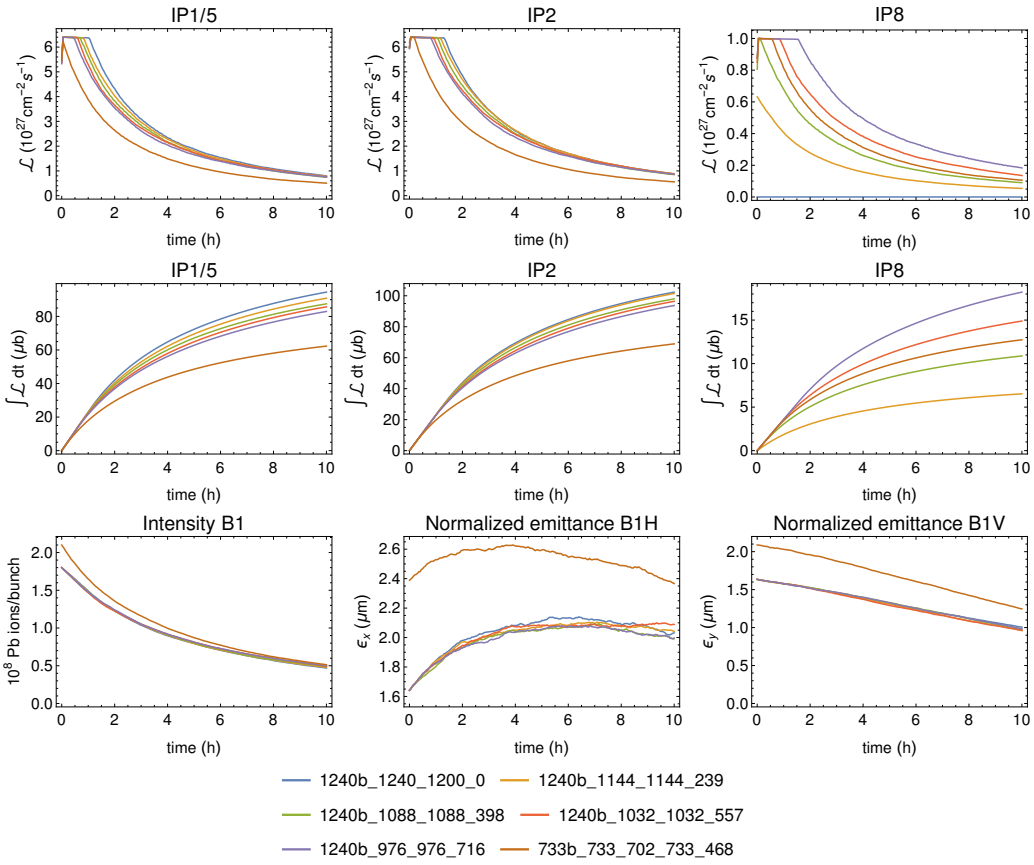

Figure 9: The simulated HL-LHC Pb-Pb performance from CTE in terms of instantaneous luminosity (top) and integrated luminosity (middle) during a typical fill for the filling schemes in Table 3, shown together with the evolution of the beam intensity and normalized emittances (bottom). Only B1 is shown, but B2 is fully symmetric.

The factor η in (3) is the *operational efficiency*, which should account for downtime and unavailability of the machine, premature fill aborts, occasional longer $T_{\rm ta}$ and, most importantly, the build-up of performance to the ideal during the few weeks of the run. Conventionally, and conservatively, we take $\eta = 0.5$, as for HL-LHC proton operation [24]. In the 2018 heavy-ion run a higher η was achieved, when the machine availability was exceptionally 85% after the initial commissioning [7]. Note that η takes account of the build-up of luminosity that occurs during these short runs and is therefore less than the machine availability. Note also that $\eta = 0.5$ has been typical during some proton runs.

The calculated $\mathcal{L}_{\rm tot}$ per one-month run using these parameters and assumptions is shown in Table 10. Results without brackets are based on CTE, but corres-

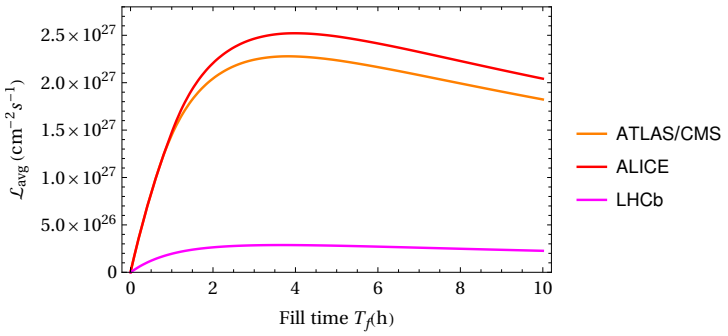

Figure 10: The time-averaged luminosity as a function of the turnaround time, calculated with Eq. (3) and the CTE simulations in Fig. 9 for the 1240b_1088_1088_398 filling scheme.

ponding MBS simulations have also been performed and these results are shown in square brackets. The two simulation codes, based on fundamentally different models, agree very well, which strengthens our confidence in the results.

For the 50 ns schemes, $\mathcal{L}_{\rm tot}$ varies in the range 2.2–2.6 nb^{-1} for ATLAS and CMS, and in the range of 2.4–2.8 nb^{-1} for ALICE[10]. The ALICE value is larger mainly due to the smaller net crossing angle. With the backup 75 ns scheme (last row in Table 10), the loss in $\mathcal{L}_{\rm tot}$ at these experiments is about 20–30% per run.

At LHCb, $\mathcal{L}_{\rm tot}$ depends strongly on the filling scheme. With the highest number of collisions considered for 50 ns beams, about 0.5 nb^{-1} can be collected per run. This is significantly higher than the 0.35 nb^{-1} for the 75 ns backup scheme 733b_733_702_468. At the same time, $\mathcal{L}_{\rm tot}$ at the other experiments is also significantly higher with 50 ns. Therefore, we conclude that the 50 ns scheme should always be preferred if available, unless it turns out to significantly degrade the other beam parameters.

4.3 Potential improvements to the Pb-Pb baseline configuration

To further increase $\mathcal{L}_{\rm tot}$, and thereby decrease the running time needed to reach the targets in Table 1, some potential improvements to the baseline scenarios are still in hand. Firstly, β^* could be squeezed to smaller values at all IPs. As discussed in Sec. 3.2, there is some margin between the protected and available aperture, as well as some potential to tighten the collimation hierarchy and further decrease the protected aperture. This comes, however, at the increased risk of losses close

[10]It should be noted that the values presented are slightly lower than in [17] because the bunch pattern is taken into account in more detail and the phenomenological 100 h non-collisional lifetime, based on measurements, has been included. The present report should be considered as an update to [17].

Filling scheme	$\mathcal{L}_{\text{tot}}$ IP1/5	$\mathcal{L}_{\text{tot}}$ IP2	$\mathcal{L}_{\text{tot}}$ IP8
1240b_1240_1200_0	2.5 [2.6]	2.7 [2.8]	0 [0]
1240b_1144_1144_239	2.4 [2.5]	2.7 [2.8]	0.18 [0.21]
1240b_1088_1088_398	2.4 [2.4]	2.6 [2.7]	0.30 [0.34]
1240b_1032_1032_557	2.3 [2.3]	2.5 [2.6]	0.39 [0.44]
1240b_976_976_716	2.2 [2.2]	2.5 [2.6]	0.46 [0.50]
733b_733_702_468	1.7 [1.8]	1.9 [1.9]	0.35 [0.36]

Table 10: Integrated luminosity (given in nb^{-1}) during a one-month Pb-Pb run at each experiment for the considered filling schemes, assuming an operational efficiency of η=0.5 h and 24 days available for physics operation in Eq. (3)–(4). The first number uses the luminosity calculated using the CTE results in Fig. 9, and the number in square brackets has been calculated using MBS.

to the experiments, and the limits in terms of feasibility of the optics matching are not known in detail. In terms of aperture, it should be noted that β^*-values down to 25 cm were used in IR1 and IR5 for protons in Run 2 [31, 35] and that a scaling of the 2018 IR2 aperture measurements [36, 37] makes it likely that $\beta^* = 0.4\,\text{m}$ can be reached there. Furthermore, when the new large-aperture triplets in IR1 and IR5 are available in Run 4, significantly smaller values of β^* are available there from the point of view of aperture. However, this would rely on an ATS optics. The question of whether an ATS squeeze in IR1/5 is compatible with a squeeze to $\beta^* \leq 0.5\,\text{m}$ in IR2 remains to be studied.

A reduction of β^* in IR2 is complicated by constraints on the crossing angle. The baseline net half angle of $100\,\mu$rad gives a minimum 6 σ beam-beam separation at β^*=0.5 m [25], and going down in β^* would require a larger crossing angle to keep the separation constant. However, a larger angle is not possible, since this would compromise the ZDC detector acceptance. There may be some margin to decrease the separation since a smaller separation was successfully used in operation in the 2018 proton run with more challenging 25 ns beams and a factor 8 larger bunch charge.

In IR8, the $\beta^* = 1.5\,\text{m}$ baseline at LHCb gives a large aperture margin, which could potentially be used to squeeze further. On the other hand, the IR8 crossing plane aperture has never been measured with beam. A first estimate has been made by scaling the aperture calculated in the existing $\beta^* = 1.5\,\text{m}$ optics, conservatively using the HL-LHC aperture calculation method for protons in [78]. At a constant crossing angle, a limit of $\beta^* = 0.65\,\text{m}$ is found, while a limit of $\beta^* = 0.5\,\text{m}$ is obtained if we use the tolerances based on LHC measurements [78].

To give a first idea of the potential for performance gains, a second set of CTE simulations was run, assuming optimistically $\beta^* = 0.4\,\text{m}$ in IR1, IR2, and IR5,

and $\beta^* = 0.5\,\mathrm{m}$ in IR8, while keeping the baseline crossing angles. As pointed out previously, the feasibility of such a scenario still remains to be demonstrated in detail. The results are illustrated in Fig. 11, which shows $\mathcal{L}_{\mathrm{tot}}$ per one-month run as function of the number of bunches colliding per IP, together with baseline performance from Sec. 4.2. In the configuration with smaller β^*, we observe a gain in $\mathcal{L}_{\mathrm{tot}}$ of 6–9% in ATLAS, ALICE and CMS.

For the configurations with the largest number of collisions at LHCb, the gain in $\mathcal{L}_{\mathrm{tot}}$ there is about 40%, and the gain is even higher, up to a factor 2, for configurations with fewer collisions. The gain is smaller with more collisions since LHCb is levelled. The levelling time in LHCb then goes up to around 4 h and thus becomes similar to $T_{\mathrm{f,opt}}$. This means that a further increase of the levelling time would not bring a significant increase, unless the fills are kept longer at the expense of the other experiments.

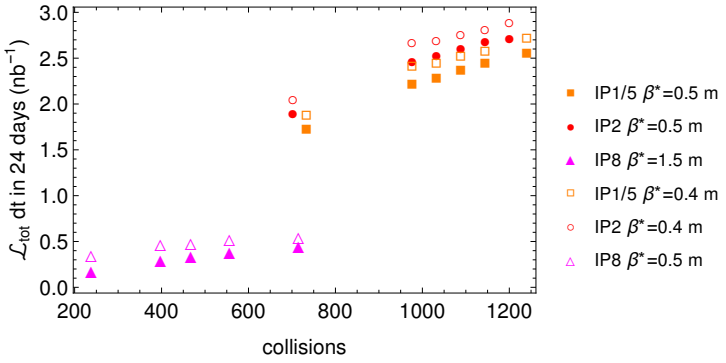

Figure 11: Calculated integrated luminosity during a one-month Pb-Pb run at each experiment for the filling schemes in Table 3 comparing the baseline configuration (filled markers) with a reduced-β^* configuration (open markers). The luminosity has been calculated using CTE simulations and Eq. (3)–(4), assuming an operational efficiency of η=0.5 and 24 days available for physics operation.

We have also investigated other performance enhancements for comparison. If the IP1/5 half crossing angle could be reduced to 100 μrad as at IP2, a gain of 6–7% at IP1/5 and a loss of 2–4% at IP2 are simulated. The crossing angle has a larger effect at IP8, where a configuration with opposite spectrometer polarity could possibly be envisaged, e.g. using an external half angle of -235 μrad and a spectrometer half angle of +135 μrad. With a net half angle of -100 μrad, a gain in $\mathcal{L}_{\mathrm{tot}}$ of around 13% is observed. It could also be envisaged not to use luminosity levelling at IP1/5, since the detectors are not limited and there is still margin to the BFPP quench limit. However, using the above assumptions the simulated gain in $\mathcal{L}_{\mathrm{tot}}$ is rather limited at about 1–2%, with a similar loss at IP2/8. In this case, $T_{\mathrm{f,opt}}$ is significantly different between IP1/5 and IP2. It could thus be envisaged

to use shorter fills with a $T_{\mathrm{f,opt}}$ calculated for IP1/5, and compensate by using a new filling scheme that redistributes some collisions to IP2. Such a scheme could potentially provide gains for all experiments, but a detailed study is left as future work.

Other ideas for performance enhancements that could be studied in the future include the use of flat optics, or the crab cavities in IR1 and IR5 that will anyway be installed for the proton runs. Finally, the operational efficiency achieved in Run 2 was better than the conservative assumption $\eta = 0.5$, meaning that there is a chance of a higher $\mathcal{L}_{\mathrm{tot}}$ per run.

In this section we have outlined several possible ways to improve the performance, however, it should be underlined that these still need to be demonstrated through further studies.

4.4 Projected performance for p-Pb

For p-Pb operation, detailed considerations are given in [60] and we give a summary here. We assume the same filling patterns as for Pb-Pb. This is an approximation, since the injection sequence for protons is different from the one for Pb. The proton injection is expected to be rather flexible. Nevertheless, to account for the possibility that the proton injection is not flexible enough to perfectly reproduce the Pb filling pattern, 5% of the total integrated luminosity is subtracted.

In the simulations, B1 is assumed to contain Pb and B2 protons, but interchanging the beams does not influence the outcome at this level. We assume the same Pb beam parameters as for Pb-Pb (see Table 4) and that the proton beam has intensities chosen to be at 3×10^{10} protons per bunch. We assume normalized proton emittances around $2.5\,\mu$m, as for p-p operation, however, there is clearly margin to decrease this due to the low intensity.

We include in MBS a phenonemological 100 h non-collisional lifetime for the Pb beam as in Sec. 4.2. In addition, as explained in [60] and based on fits to 2016 p-Pb data, an IP-dependent lifetime of 38 h is included per collision for bunches colliding in IP1 and IP5, 48 h in IP2 and 317 h in IP8. For the proton beam, a 5842 h non-collisional lifetime is used for all bunches, as observed in 2016 [60]. It is assumed that ALICE is levelled at $\mathcal{L} = 5\times10^{29}$ cm^{-2}s^{-1}, a factor 5 higher than in 2016, thanks to the ALICE upgrade [14, 15]. As in 2016, ATLAS, CMS, and LHCb are not levelled. The assumed burn-off cross sections for p-Pb are shown in Table 9. Because of their strong dependence on Z, the electromagnetic processes are almost negligible in comparison to Pb-Pb operation.

The simulated time evolution of the luminosity and beam parameters from MBS are shown in Fig. 12 for the various filling schemes in Table 3. The proton intensity remains almost unchanged as the luminosity losses are small in comparison to the total intensity. The Pb beam loses about one order of magnitude of its

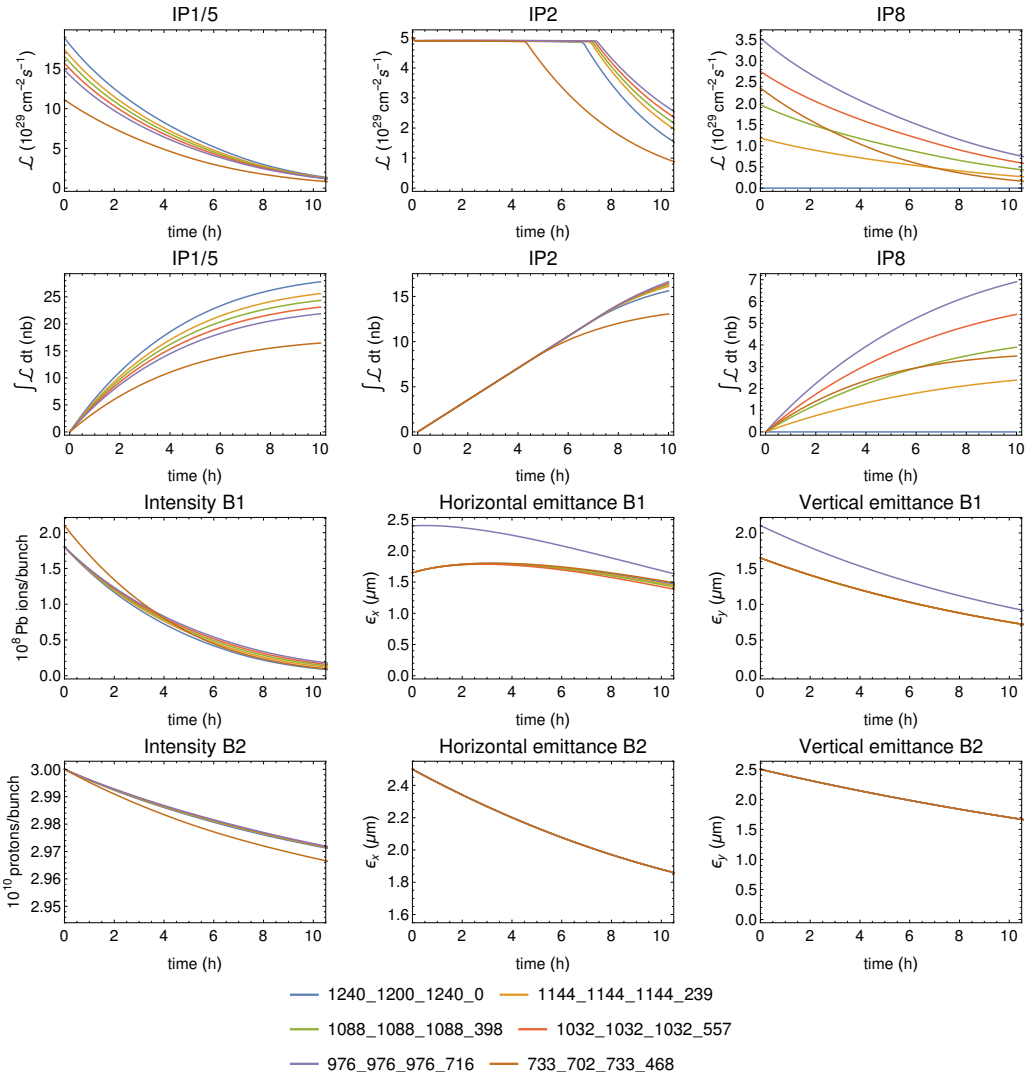

Figure 12: The simulated HL-LHC p-Pb performance from MBS in terms of instantaneous luminosity (1st row) and integrated luminosity (2nd row) during a typical fill for the filling schemes in Table 3, shown together with the evolution of the intensity and normalized emittances of the Pb ions in B1 (3rd row) and protons in B2 (4th row).

intensity in 10 h.

The ATLAS/CMS luminosity starts from a peak of $\mathcal{L}$ =22.3 $\times$ 10^{29} cm^{-2}s^{-1}, about twice what was achieved in 2016, and then decays rapidly. ALICE needs to be levelled significantly longer than with Pb-Pb, with typical levelling times of 6–7 h. The optimal fill time, calculated to maximise $\mathcal{L}_{\text{avg}}$ in Eq. (3) and assuming

Filling scheme	$\mathcal{L}_{\rm tot}$ IP1/5	$\mathcal{L}_{\rm tot}$ IP2	$\mathcal{L}_{\rm tot}$ IP8
1240b_1240_1200_0	677 [687]	306 [313]	0 [0]
1240b_1144_1144_239	634 [629]	309 [316]	45 [53]
1240b_1088_1088_398	605 [596]	308 [317]	73 [87]
1240b_1032_1032_557	583 [563]	311 [319]	103 [121]
1240b_976_976_716	558 [531]	312 [312]	135 [154]
733b_733_702_468	415 [416]	287 [294]	86 [89]

Table 11: Integrated luminosity (in nb^{-1}) during a one-month p-Pb run at each experiment for the filling schemes considered, using Eq. (3)–(4) with the assumptions explained in the text. The first value comes from CTE while the one in square brackets is from MBS using the results in Fig. 12.

$T_{\rm ta} = 200$ minutes, is therefore rather different between IP2 (typically around 8 h) and IP1/5 (typically around 4.8 h). The fill time used for the calculation of $\mathcal{L}_{\rm tot}$ is therefore estimated as the geometric mean of the two optima, typically $T_{\rm f} \approx 6.2\,\mathrm{h}$.

The calculated $\mathcal{L}_{\rm tot}$ per one-month run is given in Table 11 with the same assumptions as for Pb-Pb. Results from CTE and MBS agree to within 3% at IP1/5 and IP2. Slightly larger discrepancies af about 15% are found at IP8.

As stated above, $\mathcal{L}_{\rm tot}$ is artificially decreased by 5% to account for uncertainties in the proton filling scheme. At ATLAS and CMS, $\mathcal{L}_{\rm tot}$ is in the range of 530–690 nb^{-1} per run for the 50 ns schemes, which is significantly higher than the 310 nb^{-1} obtained at ALICE, mainly because there is no levelling. The loss in $\mathcal{L}_{\rm tot}$ with the 75 ns backup scenario is about 20–40% for ATLAS and CMS, but only about around 10% for ALICE, thanks to the levelling.

At LHCb, the maximum simulated $\mathcal{L}_{\rm tot}$ in a one-month run over the filling schemes is about 150 nb^{-1}. To reach the target in Table 1 more quickly, we could envisage improvements such as a smaller β^* at IP8, smaller crossing angle, possibly in combination with a filling scheme that displaces even more collisions from IP1/5 to IP8.

5 Conclusions

We have reviewed the running scenarios for Pb-Pb and p-Pb operation during Run 3 and Run 4. The main parameters are summarised in Appendix C. The scenarios studied rely on 50 ns Pb beams, which are constructed using slip-stacking in the SPS. In total 1240 bunches are stored in the LHC with an estimated intensity of 1.8×10^8 Pb ions per bunch. In the event that slip-stacking is not available, we consider the 75 ns scheme with 733 bunches as a backup. This worked well in 2018.

The optics baseline uses $\beta^* = 0.5\,\mathrm{m}$ in IP1, IP2, and IP5, and $\beta^* = 1.5\,\mathrm{m}$ in IP8, with no need for ATS optics. Following the upgrade of ALICE in LS2, a Pb-Pb luminosity of 6.4×10^{27} cm^{-2}s^{-1} can be taken as the levelling target for IP1, IP2, and IP5 (using separation levelling). We foresee levelling at 1×10^{27} cm^{-2}s^{-1} at IP8 to avoid the risk of quenches due to BFPP. In IR1 and IR5, the BFPP losses will be mitigated with orbit bumps as in Run 2, while the new TCLD collimators will allow higher luminosity at IP2.

In p-Pb operation, BFPP losses are not an issue so ATLAS, CMS, and LHCb will not be levelled. Luminosity debris from the Pb beam in IR1 and IR5 will be alleviated using existing TCL collimators. ALICE will be levelled at 5×10^{29} cm^{-2}s^{-1} to stay below the detector saturation.

We have estimated the luminosity performance with two independent simulation codes, based on different principles. Both agree very well with LHC data. Several filling schemes have been studied with different distributions of collisions between the experiments. We estimate an integrated luminosity per one-month Pb-Pb run of about 2.2–2.6 nb^{-1} in ATLAS and CMS, 2.4–2.8 nb^{-1} in ALICE and up to about 0.5 nb^{-1} in LHCb for the 50 ns scenarios, assuming a 50% operational efficiency and 24 days of physics operation after the initial commissioning. This would mean that about five one-month runs would be needed to reach the 13 nb^{-1} target proposed in [18].

With p-Pb, the integrated luminosity per one-month run is estimated to lie in the range of 530–690 nb^{-1} at ATLAS and CMS, and about 310 nb^{-1} at ALICE, meaning that two p-Pb runs is possibly enough to reach the targets in [18] (1.2 nb^{-1} in IP1 and IP5, 0.6 nb^{-1} in IP2). At LHCb, up to about 150 nb^{-1} is estimated per run, so the luminosity collected in two runs would still be about a factor 2 below the target of 0.6 nb^{-1}.

The present projections might be exceeded, e.g. if the operational efficiency or injected bunch intensity is higher. Other ways to gain integrated luminosity could include smaller β^*, smaller crossing angles, or modified filling schemes.

Acknowledgments

This research was supported by the HL-LHC project.

We would like to thank several colleagues for discussions and inputs: R. Alemany, G. Arduini, C. Bahamonde, E. Chapochnikova, S. Fartoukh, M. Giovannozzi, A. Lechner, and R. Tomas.

A Pb filling schemes

Below we provide details on the injection scheme for each of the considered filling patterns. The injection sequence is given per beam as a list of pairs of numbers, where the first number represents the RF bucket number of the first injected bunch in the train, and the second number represents the total number of bunches in the train to be injected.

For the 50 ns schemes, the LHC trains consists of 5 or 7 SPS trains with 8 bunches each. Inside the trains, the bunches are spaced by 50 ns, while the spacing between the SPS trains is 100 ns. An injection of 56 bunches into the LHC consists therefore of 7 SPS trains, and a 40-bunch injection consists of 5 SPS trains. More details on the beams from the SPS are given in [12].

For the 75 ns scheme, which is identical to the one used in 2018, there are 3 bunches per SPS train, spaced by 75 ns, and the spacing between the SPS trains is 300 ns. Therefore, an injection of e.g. 36 bunches consists of 12 such SPS trains. The very first injection per ring has instead only one SPS train with 4 bunches spaced by 100 ns.

- 1240b_1240_1200_0 (50 ns)
  - **B1:** (1, 56), (1541, 56), (3081, 56), (4621, 56), (6161, 56), (7701, 40), (8911, 56), (10451, 56), (11991, 56), (13531, 56), (15071, 56), (16611, 40), (17821, 56), (19361, 56), (20901, 56), (22441, 56), (23981, 56), (25521, 40), (26731, 56), (28271, 56), (29811, 56), (31351, 56), (32891, 56)
  - **B2:** (1, 56), (1541, 56), (3081, 56), (4621, 56), (6161, 56), (7701, 40), (8911, 56), (10451, 56), (11991, 56), (13531, 56), (15071, 56), (16611, 40), (17821, 56), (19361, 56), (20901, 56), (22441, 56), (23981, 56), (25521, 40), (26731, 56), (28271, 56), (29811, 56), (31351, 56), (32891, 56)
- 1240b_1144_1144_239 (50 ns)
  - **B1:** (1, 56), (1541, 56), (3081, 56), (4621, 56), (6161, 56), (7701, 40), (8911, 56), (10451, 56), (11991, 56), (13531, 56), (15071, 56), (16641, 40), (17821, 56), (19361, 56), (20901, 56), (22441, 56), (24011, 56), (25551, 40), (26731, 56), (28271, 56), (29811, 56), (31351, 56), (32921, 56)
  - **B2:** ((1, 56), (1541, 56), (3081, 56), (4621, 56), (6161, 56), (7701, 40), (8911, 56), (10451, 56), (11991, 56), (13531, 56), (15071, 56), (16611, 40), (17821, 56), (19361, 56), (20901, 56), (22441, 56), (23981, 56), (25551, 40), (26731, 56), (28271, 56), (29811, 56), (31351, 56), (32921, 56))

- 1240b_1088_1088_398 (50 ns)
  - **B1:** "(1, 56), (1541, 56), (3081, 56), (4621, 56), (6161, 56), (7701, 40), (8911, 56), (10451, 56), (11991, 56), (13531, 56), (15071, 56), (16641, 40), (17821, 56), (19361, 56), (20901, 56), (22471, 56), (24011, 56), (25551, 40), (26731, 56), (28271, 56), (29811, 56), (31381, 56), (32921, 56)
  - **B2:** (1, 56), (1541, 56), (3081, 56), (4621, 56), (6161, 56), (7701, 40), (8911, 56), (10451, 56), (11991, 56), (13531, 56), (15071, 56), (16611, 40), (17821, 56), (19361, 56), (20901, 56), (22441, 56), (23981, 56), (25551, 40), (26731, 56), (28271, 56), (29811, 56), (31381, 56), (32921, 56)
- 1240b_1032_1032_557 (50 ns)
  - **B1:** (1, 56), (1541, 56), (3081, 56), (4621, 56), (6161, 56), (7701, 40), (8911, 56), (10451, 56), (11991, 56), (13531, 56), (15071, 56), (16641, 40), (17821, 56), (19361, 56), (20931, 56), (22471, 56), (24011, 56), (25551, 40), (26731, 56), (28271, 56), (29841, 56), (31381, 56), (32921, 56)
  - **B2:** (1, 56), (1541, 56), (3081, 56), (4621, 56), (6161, 56), (7701, 40), (8911, 56), (10451, 56), (11991, 56), (13531, 56), (15071, 56), (16611, 40), (17821, 56), (19361, 56), (20901, 56), (22441, 56), (23981, 56), (25551, 40), (26731, 56), (28271, 56), (29841, 56), (31381, 56), (32921, 56)
- 1240b_976_976_716 (50 ns)
  - **B1:** (1, 56), (1541, 56), (3081, 56), (4621, 56), (6161, 56), (7701, 40), (8911, 56), (10451, 56), (11991, 56), (13531, 56), (15071, 56), (16641, 40), (17821, 56), (19391, 56), (20931, 56), (22471, 56), (24011, 56), (25551, 40), (26731, 56), (28301, 56), (29841, 56), (31381, 56), (32921, 56)
  - **B2:** (1, 56), (1541, 56), (3081, 56), (4621, 56), (6161, 56), (7701, 40), (8911, 56), (10451, 56), (11991, 56), (13531, 56), (15071, 56), (16611, 40), (17821, 56), (19361, 56), (20901, 56), (22441, 56), (23981, 56), (25551, 40), (26731, 56), (28301, 56), (29841, 56), 31381, 56), (32921, 56)
- 733b_733_702_468 (75 ns)
  - **B1:** (1, 4), (491, 36), (2191, 42), (4131, 42), (6071, 42), (8061, 21), (9161, 42), (11101, 42), (13041, 42), (14981, 42), (16971, 21), (18071, 42), (20011, 42), (21951, 42), (23891, 42), (25881, 21), (26981, 42), (28921, 42), (30861, 42), (32801, 42)

– **B2:** (1, 4), (491, 36), (2191, 42), (4131, 42), (6071, 42), (8061, 21), (9161, 42), (11101, 42), (13041, 42), (14981, 42), (16971, 21), (18071, 42), (20011, 42), (21951, 42), (23891, 42), (25881, 21), (26981, 42), (28921, 42), (30861, 42), (32801, 42)

B Collimator settings expressed using different emittances

Function	name	IR	Setting at Injection (σ)	Setting at Flat top (σ)	Setting at Collision (σ)
Primary collimator	TCP	7	5.7	5.0	5.0
Secondary collimator	TCS	7	6.7	6.5	6.5
Active absorber	TCLA	7	10.0	10.0	10.0
DS collimator	TCLD	7	out	14.0	14.0
Primary collimator	TCP3	3	8.0	15.0	15.0
Secondary collimator	TCS	3	9.3	18.0	18.0
Active absorber	TCLA	3	12.0	20.0	20.0
Tertiary collimator	TCT	1/5	13.0	15.0	9.0
Tertiary collimator	TCT	2	13.0	15.0	9.0
Tertiary collimator	TCT	8	13.0	15.0	15.0
DS collimator	TCLD	2	out	out	40.0[11]
Dump protection	TCDQ	6	8.0	7.3	7.3
Dump protection	TCSP	6	7.5	7.3	7.3

Table 12: Collimator settings at injection, at the flat top energy of $7Z$TeV, and in physics operation with Pb beams. All settings are given in units of beam σ, for a normalized reference emittance of $1.4\,\mu$m, chosen to give a geometric emittance equivalent a normalized proton emittance of $3.5\,\mu$m as usually used for LHC collimator settings.

Function	name	IR	Setting at Injection (σ)	Setting at Flat top (σ)	Setting at Collision (σ)
Primary collimator	TCP	7	5.5	4.6	4.6
Secondary collimator	TCS	7	6.4	5.9	5.9
Active absorber	TCLA	7	9.6	9.1	9.1
DS collimator	TCLD	7	out	12.8	12.8
Primary collimator	TCP3	3	7.7	13.7	13.7
Secondary collimator	TCS	3	8.9	16.5	16.5
Active absorber	TCLA	3	11.5	18.3	18.3
Tertiary collimator	TCT	1/5	12.5	13.7	8.2
Tertiary collimator	TCT	2	12.5	13.7	8.2
Tertiary collimator	TCT	8	12.5	13.7	13.7
DS collimator	TCLD	2	out	out	36.6[12]
Dump protection	TCDQ	6	7.7	6.7	6.7
Dump protection	TCSP	6	7.2	6.7	6.7

Table 13: Collimator settings at injection, at the flat top energy of $7Z$ TeV, and in physics operation with Pb beams. All settings are given in units of beam σ, for a normalized reference emittance of 1.5 μm at injection and 1.65 μm at top energy according to Tables 2 and 4.

C Summary tables HL-LHC Pb operation

	LHC design	2018	HL-LHC
Beam energy (ZTeV)	7	6.37	7
Total no. of bunches	592	733	1240
Bunch spacing (ns)	100	75	50
Bunch intensity (10^7 Pb ions)	7	21	18
Stored beam energy (MJ)	3.8	12.9	20.5
Total beam current (mA)	6.12	22.7	33.0
Normalized transverse emittance (μm)	1.5	2.3	1.65
Longitudinal emittance (eVs/charge)	2.5	2.33	2.42
RMS energy spread (10^{-4})	1.1	1.06	1.02
RMS bunch length (cm)	7.94	8.24	8.24
Peak RF voltage (MV)	16	14	14
Number of colliding bunches (IP1/5)	< 592	733	976–1240[a]
Number of colliding bunches (IP2)	592	702	976–1200[a]
Number of colliding bunches (IP8)	0	468	0–716[a]
β^* at IP1/5 (m)	0.55	0.5	0.5
β^* at IP2 (m)	0.5	0.5	0.5
β^* at IP8 (m)	10.0	1.5	1.5
half crossing, IP1/5 (μrad)	160	160	170
half crossing, IP2 (external,net) (μrad)	110,40	137,60	170,100
half crossing, IP8 (external,net) (μrad)	—	160	-170,-305
Peak luminosity, IP1/2/5 (10^{27} cm^{-2}s^{-1})	1.0	6.1	—
Levelled luminosity, IP1/5 (10^{27} cm^{-2}s^{-1})	—	—	6.4
Levelled luminosity, IP2 (10^{27} cm^{-2}s^{-1})	—	1.0	6.4
Levelled luminosity, IP8 (10^{27} cm^{-2}s^{-1})	—	1.0	1.0
Collimator settings (TCP7,TCS7,TCLA7) (σ)	7.3,8.6,12.2	5.9,6.7,11.8	5.9,6.7,11.8
Collimator settings (TCP3,TCS3,TCLA3) (σ)	17.7,21.3,23.7	17.7,21.3,23.7	17.7,21.3,23.7
Collimator settings (TCSP,TCDQ) (σ)	9.2,9.8	8.8,8.8	8.8,8.8
Collimator settings (TCT1,2,5,8) (σ)	10.2	9,9,9,15	10.6,17.7
Collimator settings (TCTLD2,7) (σ)	—	—	40,14
Protected machine aperture (σ)	10.3	11.8	11.8

[a] The values give the range over the filling schemes considered in this report.

Table 14: Pb beam parameters at the start of collisions in the LHC, as foreseen in the LHC design report (two experiments illuminated) [1], as achieved in 2018 [7, 6], and as envisaged for HL-LHC [17]. The 2018 parameters refer to typical in the fills with 75 ns. The collimator settings and apertures refer to a normalized reference Pb emittance of 1.0 μm, chosen to give a geometric emittance equivalent to a normalized 7 TeV proton emittance of 2.5 μm, as usually used for HL-LHC collimator settings.

References

[1] O. S. Brüning *et al.*, "LHC design report v.1 : The LHC main ring," *CERN-2004-003-V1*, 2004.

[2] F. Carminati *et al.*, "Alice: Physics performance report, volume i," *Journal of Physics G: Nuclear and Particle Physics*, vol. 30, no. 11, pp. 1517–1763, 2004.

[3] J. Jowett *et al.*, "First run of the LHC as a heavy-ion collider," *Proceedings of IPAC11, San Sebastian, Spain*, p. 1837, 2011. URL: http://accelconf.web.cern.ch/AccelConf/IPAC2011/papers/tupz016.pdf

[4] J.M. Jowett *et al.*, "The 2015 Heavy-Ion Run of the LHC," *Proceedings of the International Particle Accelerator Conference 2016, Busan, Korea*, p. 1493, 2016. URL: http://accelconf.web.cern.ch/AccelConf/ipac2016/papers/tupmw027.pdf

[5] J. Jowett, "Colliding Heavy Ions in the LHC," in *Proceedings, 9th International Particle Accelerator Conference (IPAC 2018): Vancouver, BC Canada, April 29-May 4, 2018*, 2018, pp. 584–589.

[6] J. Jowett *et al.*, "The 2018 Heavy-Ion Run of the LHC," *Proceedings of the 10th International Particle Accelerator Conference (IPAC2019): Melbourne, Australia, May 19-24, 2019*, p. 2258, 2019.

[7] J.M. Jowett *et al.*, "Overview of ion runs during Run 2," *Proceedings of the 9th LHC Operations Evian Workshop, Evian, France*, 2019. URL: https://indico.cern.ch/event/751857/timetable/#20190130.detailed

[8] J. M. Jowett and C. Carli, "The LHC as a proton-nucleus collider," *Proc. of the European Particle Accelerator Conf. 2006, Edinburgh, Scotland*, p. 550, 2006.

[9] J.M. Jowett *et al.*, "Proton-nucleus Collisions in the LHC," *Proceedings of IPAC13, Shanghai, China*, p. 49, 2013. URL: https://cds.cern.ch/record/1572994?ln=en

[10] R. Versteegen *et al.*, "Operating the LHC Off-momentum for p-Pb Collisions," *Proceedings of IPAC13, Shanghai, China*, 2013. URL: http://accelconf.web.cern.ch/AccelConf/IPAC2013/papers/tupfi041.pdf

[11] J. Jowett *et al.*, "the 2016 proton-nucleus run of the LHC," *Proceedings of the International Particle Accelerator Conference 2017, Copenhagen, Denmark*, p. 2071, 2017. URL: http://accelconf.web.cern.ch/AccelConf/ipac2017/papers/tupva014.pdf

[12] J. Coupard *et al.*, "LHC Injectors Upgrade, Technical Design Report, Vol. II: Ions," CERN, Geneva, Tech. Rep. CERN-ACC-2016-0041, Apr 2016. URL: https://cds.cern.ch/record/2153863

[13] G. Apollinari *et al.*, *High-Luminosity Large Hadron Collider (HL-LHC): Technical Design Report V. 0.1*, ser. CERN Yellow Reports: Monographs. CERN-2017-007-M. Geneva: CERN, 2017. URL: https://cds.cern.ch/record/2284929

[14] B. Abelev *et al*, "Upgrade of the ALICE experiment: Letter of intent," *Journal of Physics G: Nuclear and Particle Physics*, vol. 41, no. 8, p. 087001, jul 2014. URL: https://doi.org/10.1088%2F0954-3899%2F41%2F8%2F087001

[15] B. Abelev *et al*, "Technical design report for the upgrade of the ALICE inner tracking system," *Journal of Physics G: Nuclear and Particle Physics*, vol. 41, no. 8, p. 087002, jul 2014. URL: https://doi.org/10.1088%2F0954-3899%2F41%2F8%2F087002

[16] J. Jowett, "HL-LHC heavy-ion beam parameters at LHC injection," *CERN EDMS 1525065*, 2015. URL: https://edms5.cern.ch/document/1525065/1.0

[17] J. Jowett, R. Alemany, M. Schaumann, P. Hermes, and T. Mertens, "HL-LHC beam parameters and performance with heavy ions—an update," *Presentation in the LHC Performance Workshop (Chamonix 2017), Chamonix, France*, 2017. URL: https://indico.cern.ch/event/580313/timetable/

[18] Z. Citron *et al.*, "Future physics opportunities for high-density QCD at the LHC with heavy-ion and proton beams," *HL/HE-LHC Workshop: Workshop on the Physics of HL-LHC, and Perspectives at HE-LHC Geneva, Switzerland, June 18-20, 2018, CERN-LPCC-2018-07*, 2018. URL: https://cds.cern.ch/record/2650176?ln=en

[19] H. Bartosik, M. Meddahi, and G. Rumolo, "LIU baseline for ions," *Presentation in the LHC Performance Workshop (Chamonix 2017), Chamonix, France*, 2017. URL: https://indico.cern.ch/event/580313/timetable/

[20] H. Bartosik *et al.*, "Injectors beam performance evolution during Run 2," *Proceedings of the 9th LHC Operations Evian Workshop, Evian, France*, 2019. URL: https://indico.cern.ch/event/751857/timetable/#20190130.detailed

[21] R. Bruce, J. M. Jowett, M. Blaskiewicz, and W. Fischer, "Time evolution of the luminosity of colliding heavy-ion beams in BNL Relativistic Heavy Ion Collider and CERN Large Hadron Collider," *Phys. Rev. ST Accel. Beams*, vol. 13, p. 091001, Sep 2010.

[22] S. Fartoukh, "Achromatic telescopic squeezing scheme and application to the LHC and its luminosity upgrade," *Phys. Rev. ST Accel. Beams*, vol. 16, p. 111002, 2013.

[23] S. Fartoukh, "LHC cycle for the 2018 ion run," *presentation in the HSS section meeting, 2018.03.14*, 2018. URL: https://indico.cern.ch/event/708091/

[24] S. Antipov *et al.*, "Update of the HL-LHC operational scenarios for proton operation," *CERN-ACC-NOTE-2018-0002*, Jan 2018. URL: https://cds.cern.ch/record/2301292

[25] J.M. Jowett, M. Schaumann, and R. Versteegen, "Heavy ion operation from run 2 to HL-LHC," *Proceedings of the Review of LHC & Injector Upgrade Plans Workshop (RLIUP)*, 2013. URL: https://indico.cern.ch/event/260492/contributions/1592075/attachments/459741/637102/JJ_5_04.pdf

[26] C. Bracco *et al.*, "TCLIA.4R2.B1 modifications," *CERN EDMS 1936597, LHC-TC-EC-0011*, 2018.

[27] R.W. Assmann, "Collimators and Beam Absorbers for Cleaning and Machine Protection," *Proceedings of the LHC Project Workshop - Chamonix XIV, Chamonix, France*, p. 261, 2005.

[28] R.W. Assmann *et al.*, "The Final Collimation System for the LHC," *Proc. of the European Particle Accelerator Conference 2006, Edinburgh, Scotland*, p. 986, 2006.

[29] R. Bruce *et al.*, "Simulations and measurements of beam loss patterns at the CERN Large Hadron Collider," *Phys. Rev. ST Accel. Beams*, vol. 17, p. 081004, Aug 2014. URL: http://link.aps.org/doi/10.1103/PhysRevSTAB.17.081004

[30] R. Bruce, R. W. Assmann, and S. Redaelli, "Calculations of safe collimator settings and β^* at the CERN Large Hadron Collider," *Phys. Rev. ST Accel. Beams*, vol. 18, p. 061001, Jun 2015. URL: http://link.aps.org/doi/10.1103/PhysRevSTAB.18.061001

[31] R. Bruce *et al.*, "Reaching record-low β^* at the CERN Large Hadron Collider using a novel scheme of collimator settings and optics," *Nucl. Instrum. Methods Phys. Res. A*, vol. 848, pp. 19 – 30, Jan 2017. URL: http://www.sciencedirect.com/science/article/pii/S0168900216313092

[32] R. Bruce *et al.*, "Sources of machine-induced background in the ATLAS and CMS detectors at the CERN Large Hadron Collider," *Nucl. Instrum. Methods Phys. Res. A*, vol. 729, no. 0, pp. 825 – 840, 2013.

[33] R. Bruce *et al.*, "Collimation-induced experimental background studies at the CERN Large Hadron Collider," *Phys. Rev. Accel. Beams*,

vol. 22, p. 021004, Feb 2019. URL: https://link.aps.org/doi/10.1103/PhysRevAccelBeams.22.021004

[34] N. Fuster-Martinez *et al.*, "Performance of the collimation system during the 2018 lead ion run at the Large Hadron Collider," *Proceedings of the 10th International Particle Accelerator Conference (IPAC2019): Melbourne, Australia, May 19-24, 2019*, p. 677, 2019.

[35] R. Bruce, N. Fuster-Martinez, A. Mereghetti, D. Mirarchi, and S. Redaelli, "Machine configuration," *Proceedings of the 9th LHC Operations Evian Workshop, Evian, France*, 2019. URL: https://indico.cern.ch/event/751857/timetable/#20190130.detailed

[36] "E-logbook 2018.11.04," http://elogbook.cern.ch/eLogbook/eLogbook.jsp?shiftId=1104874.

[37] "E-logbook 2018.11.07," http://elogbook.cern.ch/eLogbook/eLogbook.jsp?lgbk=60&date=20181107&shift=1.

[38] H.H. Braun *et al.*, "Collimation of Heavy Ion Beams in the LHC," *Proc. of the European Particle Accelerator Conf. 2004, Lucerne, Switzerland*, p. 551, 2004.

[39] R. Bruce *et al.*, "Measurements of heavy ion beam losses from collimation," *Phys. Rev. ST Accel. Beams*, vol. 12, no. 1, p. 011001, Jan 2009.

[40] P. Hermes *et al.*, "Measured and simulated heavy-ion beam loss patterns at the CERN Large Hadron Collider," *Nucl. Instrum. Methods Phys. Res. A*, vol. 819, pp. 73 – 83, Feb 2016. URL: https://www.sciencedirect.com/science/article/pii/S0168900216002175?via%3Dihub

[41] P. Hermes, "Heavy-Ion Collimation at the Large Hadron Collider : Simulations and Measurements," Ph.D. dissertation, University of Munster, 2016.

[42] P. Hermes *et al.*, "LHC Heavy-Ion Collimation Quench Test at 6.37Z TeV," *CERN-ACC-NOTE-2016-0031*, Mar 2016. URL: http://cds.cern.ch/record/2136828

[43] A. Waets *et al.*, "Updated energy deposition simulations in ds," *Presentation at the 9th HL-LHC Collaboration meeting, Fermilab, USA*, 2019. URL: https://indico.cern.ch/event/806637/contributions/3574823/

[44] D. Mirarchi, "Crystal Collimation for LHC," Ph.D. dissertation, Imperial College, London, Aug 2015. URL: http://cds.cern.ch/record/2036210

[45] W. Scandale *et al.*, "Observation of channeling for 6500 GeV/c protons in the crystal assisted collimation setup for LHC," *Physics Letters B*, vol. 758, pp. 129 – 133, 2016. URL: http://www.sciencedirect.com/science/article/pii/S0370269316301514

[46] D. Mirarchi, G. Hall, S. Redaelli, and W. Scandale, "Design and implementation of a crystal collimation test stand at the large hadron collider," *The European Physical Journal C*, vol. 77, no. 6, p. 424, Jun 2017. URL: https://doi.org/10.1140/epjc/s10052-017-4985-4

[47] S. R. Klein, "Localized beampipe heating due to e- capture and nuclear excitation in heavy ion colliders," *Nucl. Inst. & Methods A*, vol. 459, p. 51, 2001.

[48] J. M. Jowett, J. B. Jeanneret, and K. Schindl, "Heavy Ion Beams in the LHC," *Proc. of the Particle Accelerator Conf. 2003, Portland*, p. 1682, 2003.

[49] J. M. Jowett *et al.*, "Limits to the Performance of the LHC with Ion Beams," *Proc. of the European Particle Accelerator Conf. 2004, Lucerne*, p. 578, 2004.

[50] R. Bruce *et al.*, "Observations of beam losses due to bound-free pair production in a heavy-ion collider," *Phys. Rev. Letters*, vol. 99, no. 14, p. 144801, 2007. URL: https://link.aps.org/doi/10.1103/PhysRevLett.99.144801

[51] R. Bruce, D. Bocian, S. Gilardoni, and J. M. Jowett, "Beam losses from ultraperipheral nuclear collisions between Pb ions in the Large Hadron Collider and their alleviation," *Phys. Rev. ST Accel. Beams*, vol. 12, no. 7, p. 071002, Jul 2009.

[52] M. Schaumann, "Heavy-ion performance of the LHC and future colliders," Ph.D. dissertation, RWTH Aachen, Germany, Oct 2015. URL: https://cds.cern.ch/record/2065692

[53] A. J. Baltz, M. J. Rhoades-Brown, and J. Weneser, "Heavy-ion partial beam lifetimes due to coulomb induced processes," *Phys. Rev. E*, vol. 54, p. 4233, 1996.

[54] H. Meier, Z. Halabuka, K. Hencken, D. Trautmann, and G. Baur, "Bound-free electron-positron pair production in relativistic heavy-ion collisions," *Phys. Rev. A*, vol. 63, no. 3, p. 032713, 2001.

[55] M. Schaumann *et al.*, "LHC BFPP Quench Test with Ions (2015)," *CERN-ACC-NOTE-2016-0024*, 2016. URL: https://cds.cern.ch/record/2127951?ln=en

[56] J.M. Jowett *et al.*, "Bound-free pair production in LHC Pb-Pb operation at 6.37 Z TeV per beam," *Proceedings of the International Particle Accelerator Conference 2016, Busan, Korea*, p. 1497, 2016. URL: https://cds.cern.ch/record/2207380?ln=en

[57] H. H. Braun *et al.*, "Hadronic and electromagnetic fragmentation of ultrarelativistic heavy ions at LHC," *Phys. Rev. ST Accel. Beams*, vol. 17, p.

021006, Feb 2014. URL: https://link.aps.org/doi/10.1103/PhysRevSTAB.17.021006

[58] C. Bahamonde-Castro *et al.*, "Power Deposition in LHC Magnets Due to Bound-Free Pair Production in the Experimental Insertions," *Proceedings of the International Particle Accelerator Conference 2016, Busan, Korea*, p. 1418, 2016. URL: http://accelconf.web.cern.ch/AccelConf/ipac2016/papers/tupmw006.pdf

[59] A. Lechner *et al.*, "Cleaning upgrades in the dispersion suppressors," *Presentation in the LHC collimation review 2019*, 2019. URL: https://indico.cern.ch/event/780182/contributions/3264116/

[60] M.A.Jebramcik, "Beam Dynamics of Proton-Nucleus Collisions in the Large Hadron Collider," Ph.D. dissertation, Johann Wolfgang Goethe-Universität, Frankfurt am Main, Germany, 2019.

[61] N. Mounet, "Ions are forever - a glimpse into the stability of lead ions for Run III and HL-LHC," *presentation in the HSC section meeting, 2020.03.09*, 2020. URL: https://indico.cern.ch/event/890276/

[62] N. Mounet, "Vlasov solvers and macroparticle simulations," in *Proc. ICFA Mini-Workshop on Impedances and Beam Instabilities in Particle Accelerators, Benevento, Italy, 18–22 September 2017*, ser. CERN Yellow Reports: Conference Proceedings, V. Brancolini, G. Rumolo, M. R. Masullo, and S. Petracca, Eds., vol. 1. CERN, Geneva, 2018, pp. 77–85. URL: https://doi.org/10.23732/CYRCP-2018-001.77

[63] E. Métral and A. Verdier, "Stability Diagram for Landau Damping with a Beam Collimated at an Arbitrary Number of Sigmas," 2004, cERN-AB-2004-019-ABP. URL: https://cds.cern.ch/record/733611/files/ab-2004-019.pdf

[64] X. Buffat *et al.*, "Transverse Instabilities," *Proceedings of the 9th Evian Workshop, Evian, France*, 2019. URL: https://indico.cern.ch/event/751857/

[65] D. Quartullo *et al.*, "Update on the simulations and measurements of the LHC crystal goniometer TCPCH," *presentation in the impedance working group meeting, 2019.08.02*, 2020. URL: https://indico.cern.ch/event/890276/

[66] H. Timko *et al.*, "Longitudinal dynamics," *Proceedings of the 9th LHC Operations Evian Workshop, Evian, France*, 2019. URL: https://indico.cern.ch/event/751857/timetable/#20190130.detailed

[67] T. Mertens, "Intrabeam scattering in the LHC," Master's thesis, University of Porto, 2011, presented 17 Jun 2011. URL: http://cds.cern.ch/record/1364596?ln=en

[68] S. Nagaitsev, "Intrabeam scattering formulas for fast numerical evaluation," *Phys. Rev. ST Accel. Beams*, vol. 8, no. 6, p. 064403, 2005.

[69] J. M. Jowett, "Filling schemes, collision schedules, and beam-beam equivalence classes," *Workshop on Beam-Beam Effects in Large Hadron Colliders, Geneva, Switzerland, 12 - 17 Apr 1999*, p. 63, 1999. URL: http://cds.cern.ch/record/488278

[70] K. Kubo, S. K. Mtingwa, and A. Wolski, "Intrabeam scattering formulas for high energy beams," *Phys. Rev. ST Accel. Beams*, vol. 8, p. 081001, Aug 2005. URL: https://link.aps.org/doi/10.1103/PhysRevSTAB.8.081001

[71] S. K. Mtingwa, "A new high energy approximation of intrabeam scattering for flat electron and positron beams," *African Physical Review*, vol. 2, p. 1, 2008. URL: http://aphysrev.ictp.it/index.php/aphysrev/article/view/71/34

[72] T. Persson *et al.*, "Run 2 Optics and Corrections," *Proceedings of the 9th LHC Operations Evian Workshop, Evian, France*, 2019. URL: https://indico.cern.ch/event/751857/timetable/#20190130.detailed

[73] J. Wenninger, "ALICE missing luminosity observations," *presentation in the LHC Machine Committee (LMC), 2018.11.21*, 2018. URL: https://indico.cern.ch/event/775384/contributions/3222895/attachments/1756906/2848841/LMC.LBOC-ALICElumi.21Nov18.pdf

[74] I. A. Pshenichnov, J. P. Bondorf, I. N. Mishustin, A. Ventura, and S. Masetti, "Mutual heavy ion dissociation in peripheral collisions at ultrarelativistic energies," *Phys. Rev. C*, vol. 64, no. 2, p. 024903, Jul 2001.

[75] A. J. Baltz, "Coherent heavy ion reactions," *BNL-66644*, 1999.

[76] C. Loizides, J. Kamin, and D. d'Enterria, "Improved monte carlo glauber predictions at present and future nuclear colliders," *Phys. Rev. C*, vol. 97, p. 054910, May 2018. URL: https://link.aps.org/doi/10.1103/PhysRevC.97.054910

[77] F. Alessio, private communication.

[78] R. Bruce *et al.*, "Updated parameters for HL-LHC aperture calculations for proton beams," *CERN-ACC-2017-0051*, 2017. URL: https://cds.cern.ch/record/2274330?ln=en